REPORT NO. FAA-RD-77-11

AUTOMATIC TRACKING OF WAKE VORTICES USING GROUND-WIND SENSOR DATA

John J. Deyst, Jr.
Saul Serben

The Charles Stark Draper Laboratory, Inc.
555 Technology Square
Cambridge, Ma. 02139

NAPTS
LIBRARY
JUL 25 '78

January 3, 1977

FINAL REPORT

DOCUMENT IS AVAILABLE TO THE U.S. PUBLIC THROUGH THE NATIONAL TECHNICAL INFORMATION SERVICE, SPRINGFIELD, VIRGINIA 22161

Prepared for
U.S. DEPARTMENT OF TRANSPORTATION
FEDERAL AVIATION ADMINISTRATION
Systems Research and Development Service
Washington DC 20591

NOTICE

This document is disseminated under the sponsorship of the Department of Transportation in the interest of information exchange. The United States Government assumes no liability for its contents or use thereof.

NOTICE

The United States Government does not endorse products or manufacturers. Trade or manufacturers' names appear herein solely because they are considered essential to the object of this report.

TECHNICAL REPORT STANDARD TITLE PAGE

1. Report No. FAA-RD-77-11	2. Government Accession No.	3. Recipient's Catalog No.
4. Title and Subtitle AUTOMATIC TRACKING OF WAKE VORTICES USING GROUND-WIND SENSOR DATA		5. Report Date January 3, 1977
		6. Performing Organization Code
7. Author(s) John J. Deyst, Jr., and Saul Serben		8. Performing Organization Report No. R-1009
9. Performing Organization Name and Address The Charles Stark Draper Laboratory, Inc.* 555 Technology Square Cambridge, MA 02139		10. Work Unit No. FA705/R7126
		11. Contract or Grant No. DOT-TSC-1024
12. Sponsoring Agency Name and Address U.S. Department of Transportation Federal Aviation Administration System Research and Development Service Washington, D.C. 20591		13. Type of Report and Period Covered FINAL REPORT May 1975 — April 1976
		14. Sponsoring Agency Code

15. Supplementary Notes

*Under contract to: U.S. Department of Transportation, Transportation Systems Center, Kendall Square, Cambridge, MA 02142

16. Abstract

Algorithms for automatic tracking of wake vortices using ground-wind anemometer data are developed. Methods of bad-data suppression, track initiation, and track termination are included. An effective sensor-failure detection-and-identification system is also documented. System performance is verified using actual sensor data provided by DOT/TSC. Computer requirements for implementing the system in the field are summarized, and a plan for developing a general-purpose vortex-tracking simulation is presented.

17. Key Words Suggested by Author Vortex, Tracking, Estimation, Failure Detection, Wake Vortex, Wake Turbulence		18. Distribution Statement DOCUMENT IS AVAILABLE TO THE U.S. PUBLIC THROUGH THE NATIONAL TECHNICAL INFORMATION SERVICE, SPRINGFIELD, VIRGINIA 22161	
19. Security Classif. (of this report) UNCLASSIFIED	20. Security Classif. (of this page) UNCLASSIFIED	21. No. of Pages 98	22. Price

PREFACE

This document represents the final report under Contract DOT-TSC-1024. The work was performed by personnel of The Charles Stark Draper Laboratory, Inc., Cambridge, Massachusetts. The primary purpose of the effort was to automate the reduction of data from ground-wind sensors for the purpose of tracking aircraft trailing vortices.

The authors are especially grateful to J. N. Hallock and B. Winston, of DOT/TSC for providing essential information, guidance and support during the course of the effort.

METRIC CONVERSION FACTORS

Approximate Conversions to Metric Measures

Symbol	When You Know	Multiply by	To Find	Symbol
		LENGTH		
in	inches	2.5	centimeters	cm
ft	feet	30	centimeters	cm
yd	yards	0.9	meters	m
mi	miles	1.6	kilometers	km
		AREA		
in^2	square inches	6.5	square centimeters	cm^2
ft^2	square feet	0.09	square meters	m^2
yd^2	square yards	0.8	square meters	m^2
mi^2	square miles	2.6	square kilometers	km^2
	acres	0.4	hectares	ha
		MASS (weight)		
oz	ounces	28	grams	g
lb	pounds	0.45	kilograms	kg
	short tons (2000 lb)	0.9	tonnes	t
		VOLUME		
tsp	teaspoons	5	milliliters	ml
Tbsp	tablespoons	15	milliliters	ml
fl oz	fluid ounces	30	milliliters	ml
c	cups	0.24	liters	l
pt	pints	0.47	liters	l
qt	quarts	0.95	liters	l
gal	gallons	3.8	liters	l
ft^3	cubic feet	0.03	cubic meters	m^3
yd^3	cubic yards	0.76	cubic meters	m^3
		TEMPERATURE (exact)		
°F	Fahrenheit temperature	5/9 (after subtracting 32)	Celsius temperature	°C

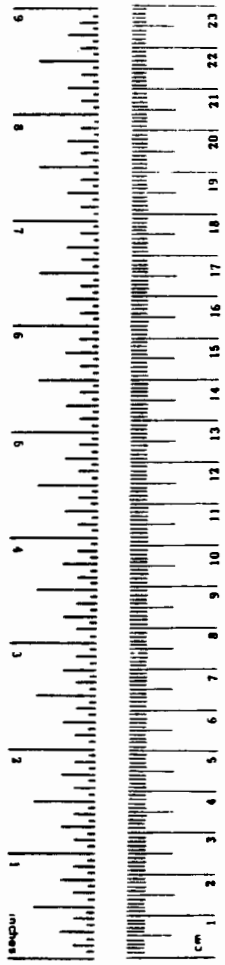

Approximate Conversions from Metric Measures

Symbol	When You Know	Multiply by	To Find	Symbol
		LENGTH		
mm	millimeters	0.04	inches	in
cm	centimeters	0.4	inches	in
m	meters	3.3	feet	ft
m	meters	1.1	yards	yd
km	kilometers	0.6	miles	mi
		AREA		
cm^2	square centimeters	0.16	square inches	in^2
m^2	square meters	1.2	square yards	yd^2
km^2	square kilometers	0.4	square miles	mi^2
ha	hectares (10,000 m^2)	2.5	acres	
		MASS (weight)		
g	grams	0.035	ounces	oz
kg	kilograms	2.2	pounds	lb
t	tonnes (1000 kg)	1.1	short tons	
		VOLUME		
ml	milliliters	0.03	fluid ounces	fl oz
l	liters	2.1	pints	pt
l	liters	1.06	quarts	qt
l	liters	0.26	gallons	gal
m^3	cubic meters	35	cubic feet	ft^3
m^3	cubic meters	1.3	cubic yards	yd^3
		TEMPERATURE (exact)		
°C	Celsius temperature	9/5 (then add 32)	Fahrenheit temperature	°F

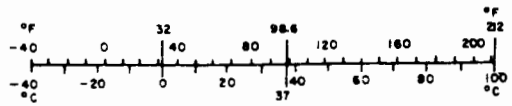

CONTENTS

Section		Page
1	INTRODUCTION	1-1
2	VORTEX TRACKER DEVELOPMENT	2-1
	2.1 Vortex Dynamics	2-1
	2.2 Simplified Vortex Transport Model	2-4
	2.3 Vortex-Induced Velocity Model	2-5
	2.4 Ground-Wind Anemometer Preprocessing	2-7
	2.5 Vortex-Tracking Estimator	2-11
	2.6 Vortex-Tracker Initialization	2-13
	2.7 Bad-Data Suppression and Tracking Quality Evaluation	2-16
	2.8 Track Termination	2-17
3	VORTEX TRACKING RESULTS	3-1
	3.1 Vortex Tracking in Calm Air	3-2
	3.2 Vortex Tracking in Strong Headwinds	3-11
	3.3 Vortex Tracking in Strong Crosswinds	3-16
	3.4 Vortex Tracking Results Summary	3-23
4	SENSOR-FAILURE IDENTIFICATION	4-1
	4.1 Sensor Bias-Failure Identification	4-2
	4.2 Sensor Noise-Failure Identification	4-3
5	COMPUTER REQUIREMENTS	5-1
	5.1 Aircraft Detection Processing and Initialization for New Aircraft Arrival	5-1
	5.2 Data-Consistency Checks and Scaling	5-1

CONTENTS (Cont.)

Section		Page
5.3	Clock-Update, Data-Output, and Executive Functions	5-2
5.4	Determination of Lateral Position of Sensors Producing Maximum Outputs	5-2
5.5	Determination of Lateral Position of Sensors Producing Minimum Outputs	5-2
5.6	Wind Computation and Vortex Propagation	5-2
5.7	Determination of Measured Starboard-Vortex Position and Estimator Update	5-2
5.8	Determination of Measured Port-Vortex Position and Estimator Update	5-2
5.9	Failure Identification	5-3
5.10	Computer Word Length	5-3
5.11	Computer Speed	5-3
6	SIMULATOR PLAN	6-1
6.1	Aircraft Module	6-1
6.2	Vortex-Dynamics Module	6-2
6.3	Sensor-Simulation Module	6-2
6.4	Tracking-System Module	6-3
6.5	Data Output-and-Display Module	6-3
6.6	Executive Program	6-3
7	CONCLUSIONS	7-1

CONTENTS (Cont.)

Section		Page
Appendix		
A	DERIVATION OF EQUATION FOR INFERRED VORTEX-POSITION MEASUREMENT	A-1
B	SUBROUTINE SUMMARIES, PROGRAM FLOWCHART, AND PROGRAM LISTINGS	B-1
C	KALMAN FILTER-GAIN EQUATIONS FOR A DOUBLE INTEGRAL PLANT	C-1
D	REPORT OF INVENTIONS	D-1
REFERENCES		R-1

ILLUSTRATIONS

Figure		Page
2.1	Typical Vortex Paths in the Presence of Steady Wind	2-3
2.2	Vortex and Ground-Wind Sensor Geometry	2-6
2.3	Typical Sensor-Indicated Velocity Pattern Caused by Vortices, Ambient Wind, and Small-Scale Turbulence, as a Function of Sensor Location	2-9
3.1a	TSC Program Output in Calm Air Using Outer Baseline Sensors with BAC Trident Vortices	3-4
3.1b	Tracking Estimator Output in Calm Air Using Outer Baseline Sensors with BAC Trident Vortices	3-4
3.2a	TSC Program Output in Calm Air Using Inner Baseline Sensors with BAC Trident Vortices	3-5
3.2b	Tracking Estimator Output in Calm Air Using Inner Baseline Sensors with BAC Trident Vortices	3-5

ILLUSTRATIONS (Cont.)

3.3a TSC Program Output in Calm Air Using Outer Baseline Sensors with DC-9 Vortices..... 3-6

3.3b Tracking Estimator Output in Calm Air Using Outer Baseline Sensors with DC-9 Vortices..... 3-6

3.4a TSC Program Output in Calm Air Using Inner Baseline Sensors with DC-9 Vortices..... 3-7

3.4b Tracking Estimator Output in Calm Air Using Inner Baseline Sensors with DC-9 Vortices..... 3-7

3.5a TSC Program Output in Calm Air Using Outer Baseline Sensors with Boeing 737 Vortices..... 3-8

3.5b Tracking Estimator Output in Calm Air Using Outer Baseline Sensors with Boeing 737 Vortices..... 3-8

3.6a TSC Program Output in Calm Air Using Inner Baseline Sensors with Boeing 737 Vortices..... 3-9

3.6b Tracking Estimator Output in Calm Air Using Inner Baseline Sensors with Boeing 737 Vortices..... 3-9

3.7a TSC Program Output in Strong Headwinds Using Outer Baseline Sensors with Boeing 727 Vortices..... 3-12

3.7b Tracking Estimator Output in Strong Headwinds Using Outer Baseline Sensors with Boeing 727 Vortices..... 3-12

3.8a TSC Program Output in Strong Headwinds Using Inner Baseline Sensors with Boeing 727 Vortices..... 3-13

3.8b Tracking Estimator Output in Strong Headwinds Using Inner Baseline Sensors with Boeing 727 Vortices..... 3-13

3.9a TSC Program Output in Strong Headwinds Using Outer Baseline Sensors with Boeing 727 Vortices..... 3-14

3.9b Tracking Estimator Output in Strong Headwinds Using Outer Baseline Sensors with Boeing 747 Vortices..... 3-14

3.10a TSC Program Output in Strong Headwinds Using Inner Baseline Sensors with Boeing 747 Vortices..... 3-15

3.10b Tracking Estimator Output in Strong Headwinds Using Inner Baseline Sensors with Boeing 747 Vortices..... 3-15

3.11a TSC Program Output in Strong Crosswinds Using Outer Baseline Sensors with Caravelle Vortices..... 3-17

3.11b Tracking Estimator Output in Strong Crosswinds Using Outer Baseline Sensors with Caravelle Vortices..... 3-17

3.12a TSC Program Output in Strong Crosswinds Using Inner Baseline Sensors with Caravelle Vortices..... 3-18

3.12b Tracking Estimator Output in Strong Crosswinds Using Inner Baseline Sensors with Caravelle Vortices... 3-18

ILLUSTRATIONS (Cont.)

		Page
3.13a	TSC Program Output in Strong Crosswinds Using Outer Baseline Sensors with Boeing 737 Vortices	3-19
3.13b	Tracking Estimator Output in Strong Crosswinds Using Outer Baseline Sensors with Boeing 737 Vortices	3-19
3.14a	TSC Program Output in Strong Crosswinds Using Inner Baseline Sensors with Boeing 737 Vortices	3-20
3.14b	Tracking Estimator Output in Strong Crosswinds Using Inner Baseline Sensors with Boeing 737 Vortices	3-20
3.15a	TSC Program Output in Strong Crosswinds Using Outer Baseline Sensors with A-300 Airbus Vortices	3-21
3.15b	Tracking Estimator Output in Strong Crosswinds Using Outer Baseline Sensors with A-300 Airbus Vortices	3-21
3.16a	TSC Program Output in Strong Crosswinds Using Inner Baseline Sensors with A-300 Airbus Vortices	3-22
3.16b	Tracking Estimator Output in Strong Crosswinds Using Inner Baseline Sensors with A-300 Airbus Vortices	3-22
6.1	Simulator Configuration	6-4

1. INTRODUCTION

The advent of very large transport aircraft with the powerful wake vortices which they produce has introduced a serious threat to smaller aircraft.[1,2,3,4,5] Numerous upsets and disturbances, because of vortex encounters, have been documented, and some serious aircraft accidents have been traced to this source. The problem is most acute on landing approach and during climbout after takeoff when flying speeds are low and precise path control is important.

An extensive theoretical and experimental vortex research program is being pursued by the U.S. Department of Transportation, Transportation Systems Center (DOT/TSC).[6,7] Results of this program have had a major impact on the basic understanding of trailing vortices. At a number of large airports, TSC has demonstrated an effective method of detecting vortices and locating their lateral positions near runways. The method uses ground-wind sensors in the form of propeller anemometers, placed in lines perpendicular to the approach path of aircraft. Software developed by TSC to postprocess data from these anemometers produces a graphical representation of probable vortex positions. However, this software is only partially automated and requires substantial manual pattern recognition and manual processing to reduce the data completely.

This report documents efforts at The Charles Stark Draper Laboratory, Inc., under contract to TSC, to automate fully the data-reduction task. The software system which has been developed processes propeller-anemometer data, and automatically tracks and records vortex position as a function of time. In addition to vortex tracking, the system also provides automatic sensor-failure detection and identification by using the multiple redundancy of sensors in the sensor lines. With minimal modification, the software can be readily adapted to provide real-time tracking in planned future wake-vortex avoidance systems.

In the following sections, the relevant aspects of the software-development effort are described. A detailed description of the basic vortex-tracking algorithm is presented. Accompanying this are descriptions of the techniques used to detect the onset of useful tracking data, to determine when useful data are no longer available, and to eliminate spurious bad data when they occur during an otherwise useful tracking period. Results of testing the algorithms, using actual sensor data gathered by the TSC system installed at London's Heathrow International Airport,[8] are explained in detail, and the character of the tracking algorithms is discussed. The methods developed for sensor-failure detection and identification are presented, and the results obtained using the Heathrow data are examined. Computer requirements to implement the software in a fielded system are summarized. Finally, a tentative plan for the future development of a simulation of a fielded vortex-tracking system is given.

2. VORTEX-TRACKER DEVELOPMENT

The vortex-tracker development is based on optimal estimation theory,[9] using appropriate mathematical models to describe vortex behavior. These models are the simplest possible descriptions which are consistent with the tracking requirements and embody only those elements which are essential to attain desired tracking performance. The following sections describe the models and the vortex tracking algorithms which were derived from them.

2.1 VORTEX DYNAMICS

At distances of five or more wingspans behind an aircraft, the flow field generated by the aircraft is approximated by two line vortices, one trailing from each wing tip. These vortices are of equal and opposite strength and are separated by a distance which is approximately equal to the aircraft wingspan. The flow field generated by each vortex is a rotational motion in which the fluid flows in concentric circles about the vortex center, so that the velocity is always tangential. At large distances from the center, the flow velocity is proportional to the vortex circulation and inversely proportional to the distance from the center. The usual expression for tangential velocity is

$$v_\theta = \frac{\Gamma}{2\pi r} , \tag{2.1}$$

where $v_\theta \equiv$ tangential velocity,

$\Gamma \equiv$ vortex circulation, and

$r \equiv$ radial distance from vortex center.

From Eq. (2.1), it is clear that as the center of the vortex is approached, the tangential velocity increases without bound. Laboratory and full-scale measurements have shown that in an actual vortex there is a region near the center where the $\frac{1}{r}$ model is invalid because the flow velocity tends to zero as the center is approached. This region is defined as the vortex core and for most aircraft of interest, the core of a newly formed vortex is smaller than about 10 feet in radius.* There is limited knowledge of the details of flow within the core and a number of models have been proposed. These models generally provide a tangential velocity field with velocity increasing monotonically with distance from the center. Parameters are chosen so that the velocity of the core model matches the velocity of the $\frac{1}{r}$ model at the radius of the core boundary. The largest uncertainties with this type of model are usually associated with judging the size of the core.

The vortex center tends to move in space according to the velocity field in which it is placed. The two vortices generated by an aircraft interact and produce vortex translational velocities which are orthogonal to the line between their centers. Distances between them are almost always many times the core size. Hence, the velocity induced by each vortex on the other is determined by Eq. (2.1) as

$$v = \frac{\Gamma}{2\pi b} , \qquad (2.2)$$

where b is the distance between the two vortices. Thus, if the two vortices generated by an aircraft are at the same altitude (i.e., the line between them is horizontal), then they translate downward at the velocity given in Eq. (2.2).

In a similar manner, if two vortices of equal and opposite strength are situated one above the other and separated by a distance d, they will move horizontally at a speed $\Gamma/2\pi d$. Furthermore, a horizontal plane of symmetry will exist half-way between the two vortices and there will be zero induced velocity across the plane. As the lower vortex is the image of the upper vortex, the flow above the plane is seen to be the same as that of a single vortex

*As the vortex ages, the core radius may grow to 30 feet or more.

of strength Γ, and at height d/2 above the ground. Hence, the ground effect produces a horizontal velocity on the vortex according to

$$v = \frac{\Gamma}{4\pi h} , \tag{2.3}$$

where h is the altitude of the vortex (i.e., half the distance to the image).

If there is wind, then the vortices also move according to the velocity of the wind field. A steady ambient wind produces a steady translation of the vortices at the ambient wind velocity.

The total effect of the interaction of the vortices with each other, influence of the ground, and influence of the wind is additive. Interaction of the two vortices with each other produces a downward motion. When the vortices pass below approximately 100 to 150 feet of altitude, depending upon vortex strength, the ground begins to affect their motion and they migrate away from each other. A steady wind tends to produce motion in the direction of the wind. The influence of the three effects on lateral vortex motions is illustrated in Figure 2.1.

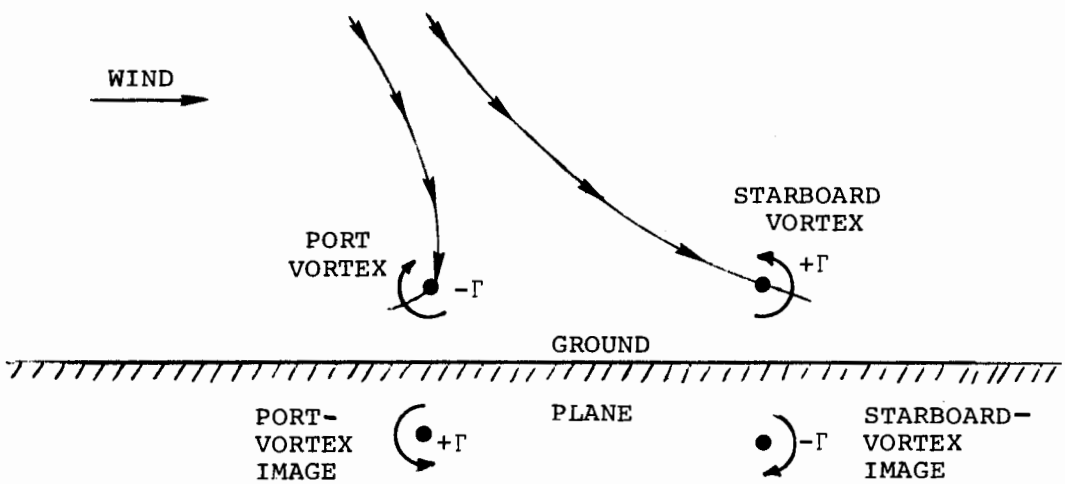

FIGURE 2.1. TYPICAL VORTEX PATHS IN THE PRESENCE OF STEADY WIND

As time passes, the vortices gradually lose their strength as the result of a number of fluid dynamic mechanisms.[10,11,12] Air turbulence is the most important mechanism promoting vortex dissipation. Small scale turbulence, of the order of the vortex core size, produces a diffusion of the vorticity resulting in a sudden "burst" of the core to an order of magnitude larger in size. Rapid decay of the vortex often follows the burst phenomenon. Turbulent eddies of a few hundred feet in scale length tend to promote a phenomenon studied by Crow[11], which distorts the line vortices into a series of ring vortices. Commonly, these ring vortices deteriorate through the "burst" mechanism described above. Under certain conditions, however, the ring vortices may persist and pose a threat to following aircraft. Very large scale turbulence tends to produce a general motion of the vortices as with ambient wind.

2.2 SIMPLIFIED VORTEX-TRANSPORT MODEL

The information for use in tracking the vortices consists of the outputs of ground-wind anemometers. Typically, they are placed a few thousand feet before the aircraft touchdown point and in lines perpendicular to the runway centerline. Following passage of an aircraft over the sensor lines, the trailing vortices descend until they begin to experience the ground effect. The onset of ground effect usually coincides with the time at which the vortices begin to have a measurable effect on the sensors; the time when useful sensor data begin to become available. Once in ground effect, the vortices separate rather rapidly, and their interactions effectively vanish. They tend to move at relatively constant velocity primarily under the influence of ground effect and wind. Thus, during the period when useful ground-wind anemometer measurements are available, the downwind vortex travels at a nearly constant velocity which is the sum of local wind and ground effect. Simultaneously, the upwind vortex also moves at nearly constant velocity, but the wind and ground effect are in opposition, and hence these effects subtract from each other (see Fig. 2.1).

The physical character of the vortex tracking problem, as described above, lends itself to a simple mathematical model for vortex motion. The basic assumption is that, during the period when the vortex produces useful sensor information, its transport velocity is relatively constant and is dominated by ambient wind and ground effect.

Defining x as the horizontal distance measured along the line of sensors from runway centerline to the vortex, the equation of vortex motion is

$$\dot{x} = u + v, \tag{2.4}$$

where $u \equiv$ ambient lateral wind velocity along the sensor line, and
$v \equiv$ the sum of vortex velocity caused by ground effect, the difference in wind velocity from ground to vortex, wind shear, and other unmodeled effects.

Typically, there are many ground-wind sensors (i.e., of the order of 20), so that the ambient ground-wind velocity u can be estimated to high accuracy. Hence, u is assumed to be a known input to the system because errors in determining u are quite small. The other velocity variable v is intended to model the remaining effects, including the difference in wind from ground level to the vortex, ground effect, and a number of other unknown, unmodeled or random effects. The equation for v is

$$\dot{v} = w, \tag{2.5}$$

where $w \equiv$ white process noise.

In other words, the variable v is a Brownian motion, and, therefore, it is characteristically an aimless, wandering type of random process. As such, it is used to account for a number of effects which are quite random in nature, or for which there is very limited knowledge in terms of accurate modeling.

2.3 VORTEX-INDUCED VELOCITY MODEL

During the period when useful data are available from the ground-wind sensors, the vortex centers are many core radii from the sensors. Hence, the $\frac{1}{r}$ flow model is appropriate to determine the component of horizontal velocity measured by the sensors. Since the sensors are at approximately ground level, ground effect is important and must be accounted for. Hence, the flow field is induced by both the actual vortex and its image. The situation is depicted in Figure 2.2. A vortex and its image each produce circular flow fields with tangential

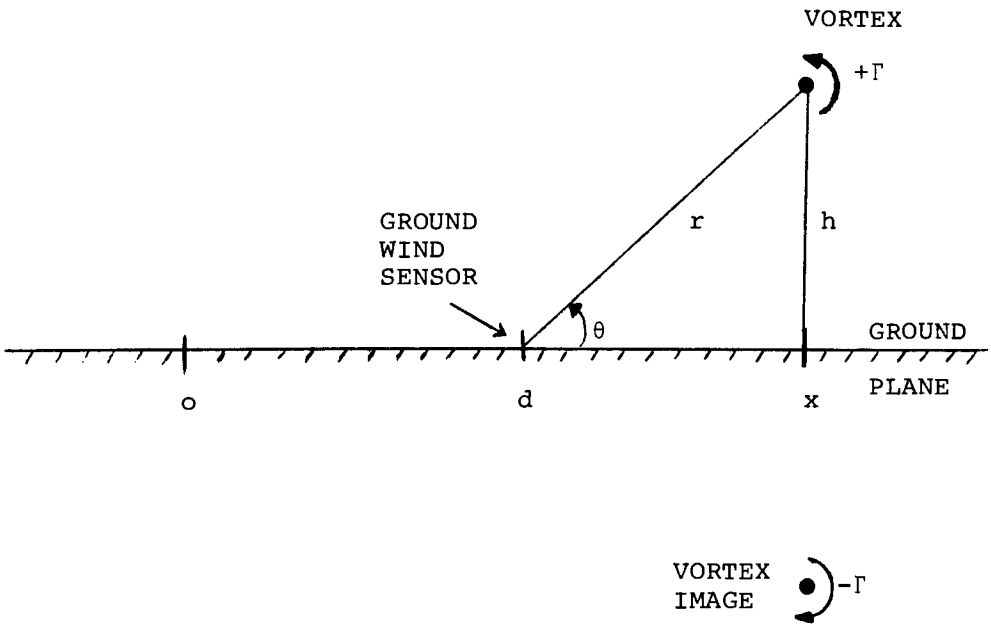

FIGURE 2.2 VORTEX AND GROUND-WIND SENSOR GEOMETRY

velocity as given in Eq. (2.1). At the ground plane, the vertical components of velocity cancel and the horizontal components add. Thus, if there is a ground-wind sensor at the point d, it measures a horizontal component of velocity given as

$$v_m = \frac{\Gamma}{\pi r}\sin\theta = \frac{h\Gamma}{\pi r^2} = \frac{\Gamma h}{\pi[h^2 + (x-d)^2]} , \qquad (2.6)$$

where θ is the elevation of the vortex relative to the ground, as measured from the sensor position, x is the lateral position of the vortex, d is the sensor location, and h is vortex altitude.

From Eq. (2.6), it is clear that the effects of the vortex on the sensor measurements are determined by three variables: circulation,

altitude, and horizontal distance from sensor to vortex. Hence, in theory, simultaneous measurements from three anemometers can determine vortex location and strength. In fact, attempting such a simultaneous solution produces rather poor estimates of vortex location. Sensor errors, modeling errors, and local wind all tend to degrade the measurements to the point where it is necessary to use another approach.

2.4 GROUND-WIND ANEMOMETER PREPROCESSING

The ground-wind anemometers, which provide the primary tracking information, are grouped in so-called sensor lines. Each line consists of about 20 sensors placed on a line orthogonal to the runway centerline. The sensors are spaced at 50-foot intervals, with the middle sensor located on the runway centerline and typically at a distance of from 1000 to 300 feet before the runway threshold. Each sensor measures the component of local air velocity which is horizontal and orthogonal to the runway centerline. Positive velocity is defined as left to right across the flight direction.

There are three primary elements which affect the sensor output: vortex-induced velocity, local wind, and sensor-instrument errors or noise. The vortex-induced velocity component is discussed in Section 2.3 and is given in Eq. (2.6). Local wind is an extremely variable phenomenon, depending primarily upon meteorological factors. For the purpose of this discussion, the wind effects will be separated into two categories depending upon the scale of turbulence in the air. One category consists of all components of local wind which are attributable to air masses of a scale which is large compared to the length of the sensor line (i.e., of scale length greater than about 1000 ft). This type of wind involves coherent motion of large masses of air, and, hence, it tends to affect all sensors in a sensor line in the same way. A steady ambient wind falls into this class. The other category consists of small-scale turbulence (i.e., of scale length less than about 1000 feet). Since this type of turbulence involves motion of masses of air which are roughly the size of the sensor line or smaller, its effect on the sensor line varies from one sensor to another. Hence, the two categories are distinguished by whether they affect all the sensors simultaneously in the same way. The final component of sensor output is the inherent measurement

error in the instrumentation itself. Typically, it consists of a bias effect and a random component, both of which are quite small if the instrument is functioning properly.

The effects of these three phenomena are additive, and they result in a pattern of sensor outputs which is typically as shown in Fig. 2.3. In Fig. 2.3, the port vortex, located at approximately +50 feet, produces a minimum in the sensor located at +50 feet, and the starboard vortex, located at approximately +325 feet, produces a maximum in the sensor located at +300 feet. Ambient wind biases the entire pattern by approximately 7 ft/sec, and small-scale turbulence produces local variations in the pattern, such as the local maximum at -350 feet and the local minimum at -200 feet.

After extensive analysis of actual sensor tracking data, it has been found that the velocities induced by vortices are only measurable over a region of about 150 to 200 feet. In other words, the effect of a vortex appears in no more than three or four sensors at a time.* For example, in Fig. 2.3 the starboard vortex only affects the sensors at 250, 300, and 350 feet. Hence, all direct information about vortex location, at any particular time, is embodied in only a few of the instruments. The remaining instruments measure the combined effect of large- and small-scale turbulence and ambient wind.

At periodic points in time, all sensor outputs are sampled almost simultaneously. This collection of 20 or so sensor outputs is preprocessed to separate the various effects of large- and small-scale turbulence from the effects of the vortices. The vortex effects manifest themselves as a local maximum and a local minimum, each of which is concentrated over two or three sensors. The regions of vortex influence are inferred by summing the outputs of pairs of adjacent sensors. The location of the pair of sensors which indicates the largest sum is used to infer the region of the starboard vortex. Similarly, the location of the pair of sensors which indicates the smallest sum is used to infer the region of the port vortex. The outputs of the sensors in each of the two pairs are then examined to choose a third sensor to accompany each pair. One sensor is chosen so that three sensor outputs associated with the starboard vortex form a convex group, and another sensor is associated with the port vortex to form a concave group. For example, in Fig. 2.3, the

*Clearly, this situation will be different for other sensor spacings.

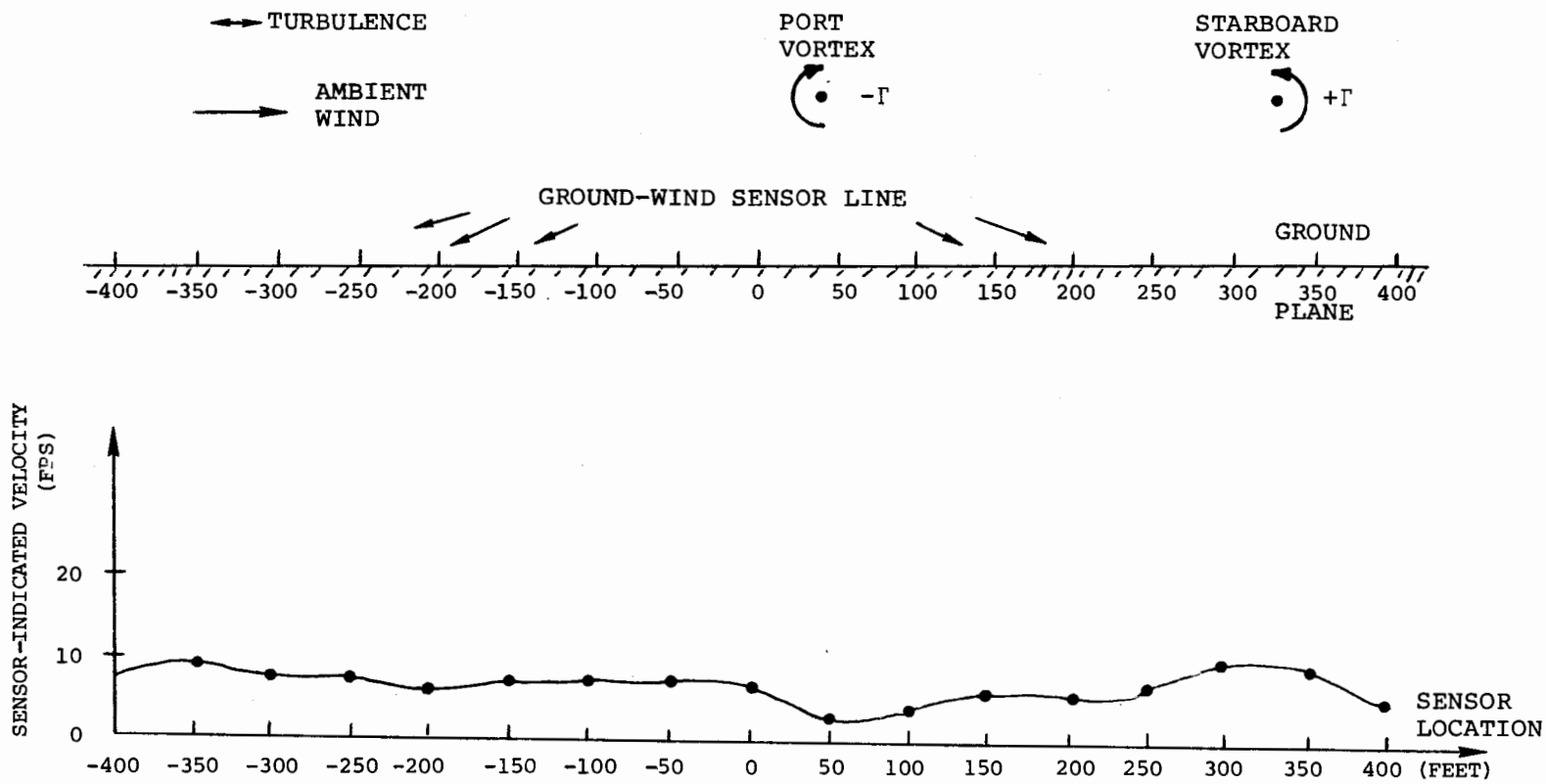

FIGURE 2.3. TYPICAL SENSOR-INDICATED VELOCITY PATTERN CAUSED BY VORTICES, AMBIENT WIND, AND SMALL-SCALE TURBULENCE AS A FUNCTION OF SENSOR LOCATION

sensors at +300 and +350 feet form the maximum sum of two, so that the starboard vortex is assumed to be nearest this pair. The sensor at +250 feet is appended to these to form a convex group of three. The starboard vortex is then assumed to be somewhere between +250 and +350 feet. Similarly, the concave group of sensors at 0, +50, and +100 feet is chosen, and the port vortex is assumed to be somewhere between 0 and 100 feet.

To determine the ambient wind, sensor outputs are averaged. However, the average does not include data from the group of three convex and the group of three concave sensors. In other words, only those sensors which are not in the region of the port and starboard vortices are included in the average. Since approximately 14 sensors remain, a relatively accurate estimate of ambient wind is thus obtained. In effect, the average does not include vortex effects. It extracts the large-scale or ambient wind effect and tends to suppress the effects of small-scale turbulence. The result is used by the estimator as a measure of the ambient wind velocity at ground level (i.e., the variable u in Eq. 2.4).

The group of three convex and the group of three concave sensor outputs are then used to infer measurements of the starboard- and port-vortex positions, respectively. First, the ambient-wind velocity, inferred from the averaging process described above, is subtracted from the outputs of the convex and concave groups of three, so as to eliminate ambient wind from the data. Then, the groups are processed to infer measured locations of the port and starboard vortices. This processing is based on the vortex induced velocity model of Section 2.3 and explained in detail in Appendix A. The formula is

$$x' = \frac{\left[v_{m_1} d_1^2 \left(v_{m_2} - v_{m_3}\right) + v_{m_2} d_2^2 \left(v_{m_3} - v_{m_1}\right) + v_{m_3} d_3^2 \left(v_{m_1} - v_{m_2}\right)\right]}{2\left[v_{m_1} d_1 \left(v_{m_2} - v_{m_3}\right) + v_{m_2} d_2 \left(v_{m_3} - v_{m_1}\right) + v_{m_3} d_3 \left(v_{m_1} - v_{m_2}\right)\right]}, \quad (2.7)$$

where x' = inferred measurement of vortex position,

v_{m_i} = velocity output of ith sensor of the group of three sensors associated with the vortex, and

d_i = location of the ith sensor.

Equation (2.7) represents the lateral position of the vortex as inferred from the outputs of the three anemometers which are likely be nearest the vortex. As described above, a number of factors corrupt the measurements and hence produce errors in inferred position. As a result, the inferred measurements are processed by vortex-tracking estimators which use a history of measurements to provide the best estimates of vortex position.

2.5 VORTEX-TRACKING ESTIMATOR

As discussed in Section 2.2 above, the vortex motion is assumed to be at almost constant velocity and characterized by Eq. 2.4 and 2.5. The horizontal distance x and transport velocity v constitute the two state variables for implementation of the estimator. Sensor outputs are sampled periodically and processed to update the estimates of these two state variables. Between measurements, the vortex motion is extrapolated in a manner which is consistent with the state-variable equations 2.4 and 2.5. Let $\hat{x}_{n-1}$ and $\hat{v}_{n-1}$ be the estimates of x and v for one of the vortices at the time step n-1, based on measurements up to and including the measurement at time n-1. Let $\tilde{x}_n$ and $\tilde{v}_n$ be the estimates of x and v at the time step n, based on measurements up to and including the measurement at n-1. Then, according to Eqs. 2.4 and 2.5 and the fact that w is a white process noise, the extrapolation from time n-1 to time n is

$$\tilde{x}_n = \hat{x}_{n-1} + (u_{n-1} + \hat{v}_{n-1})\Delta t, \tag{2.8}$$

$$\tilde{v}_n = \hat{v}_{n-1}, \tag{2.9}$$

where Δt is the time interval between n-1 and n, and u_{n-1} is the ambient ground-wind velocity determined from the ground-wind sensors, as described in Section 2.4 above.

At time n, a new set of sensor outputs is sampled. As described in Section 2.4, the measured positions of the vortices are inferred from these sensor outputs. Let x_n' be the inferred measurement of the lateral vortex position at time n. Assuming that the errors in successive inferred measurements are independent, the Kalman-filter theory is applied to this problem to yield the following update equations:

$$\hat{x}_n = \tilde{x}_n + K_{x_n}(x_n' - \tilde{x}_n), \tag{2.10}$$

$$\hat{v}_n = \tilde{v}_n + K_{v_n}(x'_n - \tilde{x}_n), \tag{2.11}$$

In effect, the extrapolated position and velocity estimates $\tilde{x}_n$ and $\tilde{v}_n$ are corrected by amounts which are proportional to the difference between the measurement x'_n and the extrapolated position estimate $\tilde{x}_n$.

The proportionality coefficients or filter gains K_{x_n} and K_{v_n} determine the character of the filter. According to the Kalman filter theory, these coefficients are determined by the statistics of the measurement errors and estimation errors. If the statistics indicate that the measurement is much more accurate than the current estimates, then the coefficients are large, giving more weight to the current measurement than to previous data. If, however, the statistics indicate that the measurement is much less accurate than the current estimate, then the coefficients are small and far less weight is given to the current measurement compared to previous data.

The estimator given in Eqs. 2.10 and 2.11 represents a second-order sampled-data system for processing measurement data. Application of the Kalman filter theory provides a direct computational method for determining the filter gains, based on the statistics of the measurement errors, the strength of the white process noise w, and the a priori statistics of the initial position and velocity of the vortex. For the problem at hand, none of these statistics are well known. Furthermore, it is likely that they change with time, so that to apply the filter theory directly, one must provide some means to infer these statistics and adjust the gains accordingly. In addition, it is important to realize that the basic system model is much simplified, and, hence, that there are inherent modeling errors.

There are a number of possible approaches which can be taken to determine appropriate filter gains. The ultimate goal is to choose gains which yield good system performance over a wide range of conditions. The term robustness has been used to characterize such systems because they are relatively insensitive to changing conditions. To calculate the gains by applying the Kalman-filter theory, one must select covariance parameters, as described above, and solve a matrix Riccati equation, the solution of which can then be used directly to obtain filter gains. The gains are thus determined by the statistics assumed when developing the Ricatti equation. Experience with many

applications of filter theory to real problems has shown that typically, for this type of filtering problem, the gains produce a well damped filter with a frequency response which balances the effects of measurement noise against initial uncertainty and the effects of process noise. With this fact known, it has been determined that the process of guessing statistics and solving the Riccati equation is a rather awkward indirect means of designing the filter. As shown in Appendix C, the damping ratio of the filter is always 0.707. Hence, it has been decided to choose K_{x_n} and K_{v_n} so that this damping ratio is always attained while allowing experimentation with the filter bandpass. This parameter is then determined by a cut-and-try process, using actual sensor data to yield a practical robust system which attains the best possible tracking performance. Thus, the basic filter configuration is the form obtained from the Kalman theory, with filter gains obtained by experimentation with actual vortex-sensor data.

Separate filters are employed for each of the two vortices, and each uses the inferred position measurement appropriate for the vortex it is tracking. For example, the starboard-vortex tracking filter uses the inferred position measurement generated from the group of three convex sensor measurements; similarly, the port-vortex tracking filter uses the group of three concave sensor measurements.

The vortex-tracking filters, as described above, have been implemented in a digital computer program and used to process data from actual ground-wind sensors installed at London's Heathrow International Airport. Appropriate gains have been chosen, and extensive testing has been done to determine the effectiveness of the trackers. In general it has been found that in relatively calm conditions, when winds are below 5 ft/sec, it is possible to choose gains which make the trackers work quite well. However, when there is appreciable wind, the trackers experience difficulty in initialization. It is apparent that they do not adapt to the wide variations in the locations of the vortices at the times when useful sensor data become available.

2.6 VORTEX-TRACKER INITIALIZATION

The tracking problem begins when an aircraft passes over the sensor line. Pressure and/or acoustic sensors are triggered by the aircraft presence,

and these signals alert the vortex-tracking system. After the aircraft passes over the sensor line, the vortices roll up and begin to descend. There is often considerable variation in the time it takes for the vortices to descend to the point where useful sensor data become available. Aircraft height, vortex strength, and meteorological conditions are all factors affecting descent time. Furthermore, the wind variations with altitude provide an additional measure of uncertainty as to vortex location when they descend.

A number of approaches have been attempted in the process of evolving a suitable initialization procedure, including adapting the initial estimates to the ambient wind, changing filter gains, and delaying the tracker initialization. None of these are totally satisfactory. Basically, the problem is one of detecting the onset of the vortex-induced velocity in the sensor measurements, and initializing the vortex-state variables (x and v) to values, so that the tracking estimator can lock onto the vortices. In effect, the onset of the starboard-vortex-induced maximum and port-vortex-induced minimum, as described in Section 2.4 and illustrated in Figure 2.3, must be detected, and the tracking estimators initialized accordingly. Hence, it has been determined that a measure of the size of the absolute minimum and absolute minimum, relative to the average sizes of local maxima and minima in the other sensors in the line would be useful. To provide this comparison, a sample standard deviation of noise in the sensor outputs is calculated at each sample time, by computing the sum of squares of sensor outputs, subtracting the square of the sum, dividing by the number of sensor outputs used and taking the square root. In this calculation the outputs of the sensors comprising the maximum sensor pair and minimum sensor pair as described in Section 2.4, are excluded. The resulting sample standard deviation is then processed through a first order low pass filter with a time constant of 6 seconds. The maximum sensor pair and the minimum sensor pair are then each divided by two, the average wind is subtracted, and the results are passed through filters which are identical to the one employed with the sample standard deviation. The resulting filtered averaged maximum sensor pair is then divided by the filtered sample standard deviation to produce a signal-to-noise ratio for the sensor data associated with the starboard vortex. Similarly, the filtered,

averaged minimum sum of two is divided by the filtered sample standard deviation to produce a signal-to-noise ratio for the sensor data associated with the port vortex. These two signal-to-noise ratios are then used to initialize the vortex-tracking filters.

Experiments with actual sensor data determined that the signal-to-noise ratios must be greater than 2.0 before useful tracking data become available. Furthermore, a delay of ten seconds after aircraft detection is imposed, during which time no initializations are made, to allow the startup transients of the low-pass filter to settle. Hence, no track initiations are done until these conditions are satisfied. However, once the delay is exceeded and a signal-to-noise ratio exceeds two, the associated filter position-state estimate $\hat{x}_n$ is initialized to the inferred position measurement x_n', and the velocity-state estimate $\hat{v}_n$ is set to zero. In effect, the filter ignores all past data, and places total faith in the current inferred position measurement, under the assumption that current data are far more important than previous data. The signal-to-noise ratios are then calculated at each succeeding measurement time, and the changes in signal-to-noise ratio, from one sample time to the next, are monitored. At each point when the new change in signal-to-noise ratio exceeds the largest change observed previously, the estimator is re-initialized. By this means, the rate of change signal-to-noise ratio is monitored, and the estimator is initialized repeatedly until the rate of change of the signal-to-noise ratio begins to decrease. This procedure is terminated at 40 seconds after aircraft detection, under the assumption that the vortices should have descended and produced significant sensor signals by that time.

As stated previously, the track-initialization procedure evolved from extensive experimentation with actual sensor data. It has been found that typically the signal-to-noise ratio builds up rapidly as the vortex descends, and then decreases gradually as the vortex dissipates. Monitoring the rate of change of signal-to-noise ratio is found be a reliable means to determine the onset of useful tracking data and an effective indicator of when to re-initialize the estimators.

2.7 BAD-DATA SUPPRESSION AND TRACKING-QUALITY EVALUATION

Experience with actual tracking data also has eliminated a problem with sensor measurement errors. At times when the signal-to-noise ratio is diminishing, random disturbances in the sensor outputs can produce very large variations in the inferred position measurement produced by the measurement preprocessing as described in Section 2.4. This problem is the result of the basically nonlinear relationship between vortex position and velocity measurements. It has been found that these large inferred measurement errors produce large perturbations in the vortex tracker, resulting in possible loss of the true vortex track by the estimator.

A straightforward and very effective remedy has been found by simply limiting the size of the corrections which can be made to the estimate. If, at the times when measurements are taken and preprocessed, the inferred measurement of vortex position differs from the extrapolated estimate of position by more than 200 feet, then the measurement is ignored and the estimate extrapolated forward without a measurement incorporation. By this device, a comparison is made between old data and new data, and if there is a large discrepency the new data are ignored. Extensive experimentation has shown that this technique, in concert with the track-initiation procedure described above, is most effective in suppressing bad data and seldom ignores good data.

A similar procedure is used when the vortices approach the boundaries of the sensor line. When this occurs, the lack of sensor data beyond the boundary can produce large errors in the sensor preprocessing procedure. Hence, once the estimated vortex track crosses a sensor-line boundary, the track is terminated.

The difference between the inferred measured position and the extrapolated estimate of position, which is often called the measurement residual, has also been found to be an effective indicator of the accuracy or quality of vortex tracking. As a means of quantifying this indicator the residual is squared at each measurement incorporation and processed through a low-pass filter. This procedure yields an approximate running evaluation of the sample mean square value of the residuals. The low-pass-filter time constant, set at 6 seconds, is long enough to provide a measure of the mean, yet short

enough to adapt readily to changing tracking conditions. The resulting tracking-quality statistic is compared against fixed threshold values to yield an evaluation of tracking quality. Letter grades are given which correspond to the magnitude of the square root of the statistic. The thresholds are set as follows:

A implies $0 < \sqrt{s} \leq 25$ ft,
B implies $25 < \sqrt{s} \leq 50$ ft,
C implies $50 < \sqrt{s} \leq 75$ ft,
D implies $75 < \sqrt{s} \leq 100$ ft,
E implies $100 < \sqrt{s} \leq 150$ ft, and
F implies $150 < \sqrt{s}$,

where s is the filtered mean-square tracking-quality statistic calculated as described above. Thus, a grade of A implies excellent tracking in the range of zero to 25 feet of error, and a grade of F implies very poor tracking with deviations larger than 150 feet.

2.8 TRACK TERMINATION

The signal-to-noise ratio and tracking-quality indicators are used to terminate vortex tracking. As the vortices age, their strength diminishes, and it is important to provide some definite indication of the end of useful tracking data. Experience has shown that typically, after the 40-second delay allowed for tracker initializations, the signal-to-noise ratio generally decreases. When the ratio falls below two and more than 40 seconds have elapsed since aircraft detection, the vortex track is terminated. Similarly, when the tracking-quality indicator falls below D, so that the rms residuals exceed 100 feet, and more than 40 seconds have elapsed since aircraft detection, then the vortex track is also terminated. These two criteria, by which track terminations are made, have been found to be effective in promptly and accurately terminating vortex tracks when useful sensor data are no longer available.

Vortex tracks are also terminated when the estimated vortex position passes beyond one of the boundaries of the sensor line. In this case, the rationale is that useful tracking data are no longer available once the vortex passes outside the line of sensors.

3. VORTEX TRACKING RESULTS

The DOT/Transportation Systems Center has installed ground-wind sensor systems at a number of airports. The vortex tracker was extensively tested with actual data tapes supplied by TSC, containing outputs from sensor lines deployed at London's Heathrow International Airport. TSC also provided vortex track printouts, from its own computer program, to be used as a reference and a standard of performance for the tracker developed at CSDL. Most of the testing was done as an integral part of the process of tracker development. Data taken on three separate days were used to test the system over a variety of tracking situations. The first data tape (HM-94) is representative of a calm day with winds generally below 10 ft/sec. The second data tape (HM-95) was recorded on a day when large headwinds were present. Finally, the third data tape (HM-62) represents a relatively high crosswind condition, when vortices are blown consistently and rapidly across the sensor line.

In the following sections, selected representative vortex tracks from these three tapes will be presented. A wide range of aircraft from Boeing 747's to BAC-111's is included. The tracking results are discussed by way of comparisons between outputs from the vortex-tracking estimator, as described above, and outputs from the tracking program developed at TSC. The TSC program indicates the locations of sensors whose outputs yield the largest number of maxima and the largest number of minima, from samples of all sensors taken at 1/7-second intervals, during successive two-second periods. Since these maxima and minima are effectively the raw data on which the vortex-tracking estimator operates, the comparisons provide a good indication of how effective the tracking estimator is in processing the raw data.

Two lines of sensors were deployed at Heathrow Airport. The so-called outer baseline was located at 2400 feet from runway threshold and it usually senses the vortices first. The inner baseline was located

closer, at 1475 feet from the threshold. Aircraft pass over the inner baseline about six seconds after passing over the outer baseline. Aircraft altitude is considerably lower over the inner baseline than is the case over the outer baseline. Hence, data from inner baseline sensors are generally of higher quality, and more effective tracking can usually be done using these data. Vortex tracks derived from both sensor baselines will be presented in the following sections.

3.1 VORTEX TRACKING IN CALM AIR

In calm air vortex tracking is relatively easy. Good tracking data are usually available within 15 seconds after the aircraft passes over a sensor line. The vortex motion is dominated by ground effect, which produces an almost constant-velocity motion of each vortex. Sensor signal-to-noise ratios are generally high, and accurate tracking is possible for long periods of time.

Figures 3.1a and 3.1b present a comparison of the outputs from the TSC program and the tracking estimator. Sensor data from Heathrow Tape HM-94 (Case 11) provide the input to the two programs. The vehicle which generated the vortices was a British Aircraft Corp. Trident airplane. The figures present data processed from sensors in the outer baseline.

Figure 3.1a is the output from the TSC program. These data can be viewed as representative of the raw data on which the vortex-tracking estimator operates. Time, designated at 10-second intervals after aircraft detection, runs vertically down the left hand edge of the figure. Distance from runway centerline is presented at intervals of 100 feet across the top of the figure. The vertical column of apostrophes in Figure 3.1a represents the runway centerline, and the columns of dots represent the edges of a corridor of ±150 feet in width, indicating the so-called protected zone for following aircraft[13]. The letter S designates the estimated location of the starboard vortex and the letter P represents the estimated location of the port vortex. In Fig. 3.1a the + sign next to a P indicates that the port vortex may lie somewhere between the P and +. Similarly a side-by-side S and * indicate a starboard-vortex location somewhere between the two.

As seen in Fig. 3.1a, good data from the port vortex appear at about 15 seconds after aircraft passage and persist until about 80

seconds, at which point the data become erratic, indicating an unreasonable discontinuous jump in port-vortex location to the right of the starboard vortex. Good tracking data on the starboard vortex appear at about 20 seconds and persist until about 95 seconds, at which point the starboard data also become erratic. The port vortex stays within the ±150 ft. region during the entire 80 second period; the starboard vortex passes beyond the +150 ft boundary at some time between 40 and 60 seconds.

The columns of letters running vertically down the left- and right-hand edges of Fig. 3.1a are measures of the confidence that can be placed in the indicated location of the vortices. For example, the letter A in the right-hand column indicates that the sensor at the location of the S, indicated in the figure at the same point in time, produced the largest output at all 14 samples taken in the preceeding two-second interval. Similarly the letter B indicates that the maximum occurred in that sensor 90-99% of the time in the preceding interval and similarly at 10% increments to F, which represents 50-59%. When fewer than 50% of the maxima occur in one sensor, the S is not printed and a blank appears in the right hand column. Similarly, the left-hand column applies to the minima which are associated with the port vortices, designated by P in the figure. All letter grades are as indicated above; however, when the minima occur less than 50% of the time in one sensor, during a two-second interval, a dash is printed in the left hand column.

Figure 3.1b presents the port and starboard tracks as indicated by the CSDL vortex-tracking estimator. The estimator calculates essentially continuous tracks to high resolution, but the figure quantizes the estimates to within 50 ft. intervals. In Figure 3.1b the column of I letters represents runway center line, lateral distances are designated in 100-ft. intervals across the top of the figure and the vertical columns of dots indicate the ±150-ft. protection region. Letters S and P indicate estimated vortex positions. The letter Q indicates a port-vortex estimator initialization, as described in Section 2.6, and T represents a starboard vortex estimator initialization. Thus, the port vortex is initialized at 16, 18, 20, 22 and 36 seconds, indicating successive increases in the rate of change of signal-to-noise ratio within the corresponding two-second intervals. The port-vortex track stays steady at about -50 ft. until 75 seconds, when it moves out to about -100 ft. The track is terminated at 80

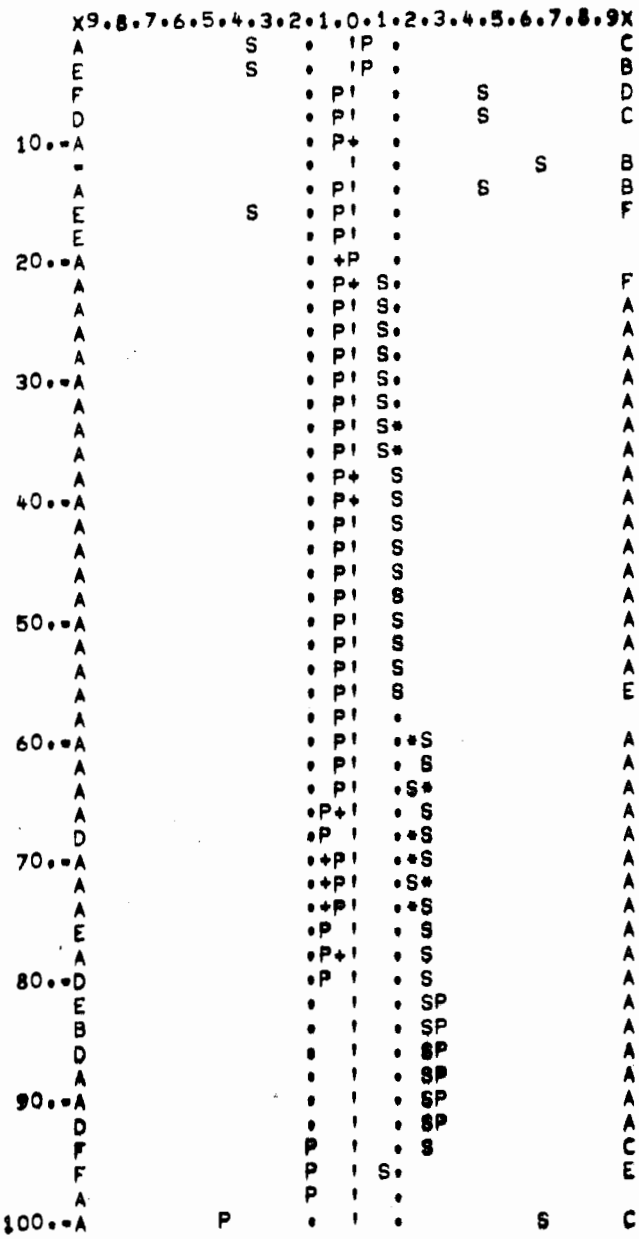

FIGURE 3.1a TSC PROGRAM OUTPUT IN CALM AIR USING OUTER BASELINE SENSORS WITH BAC TRIDENT VORTICES

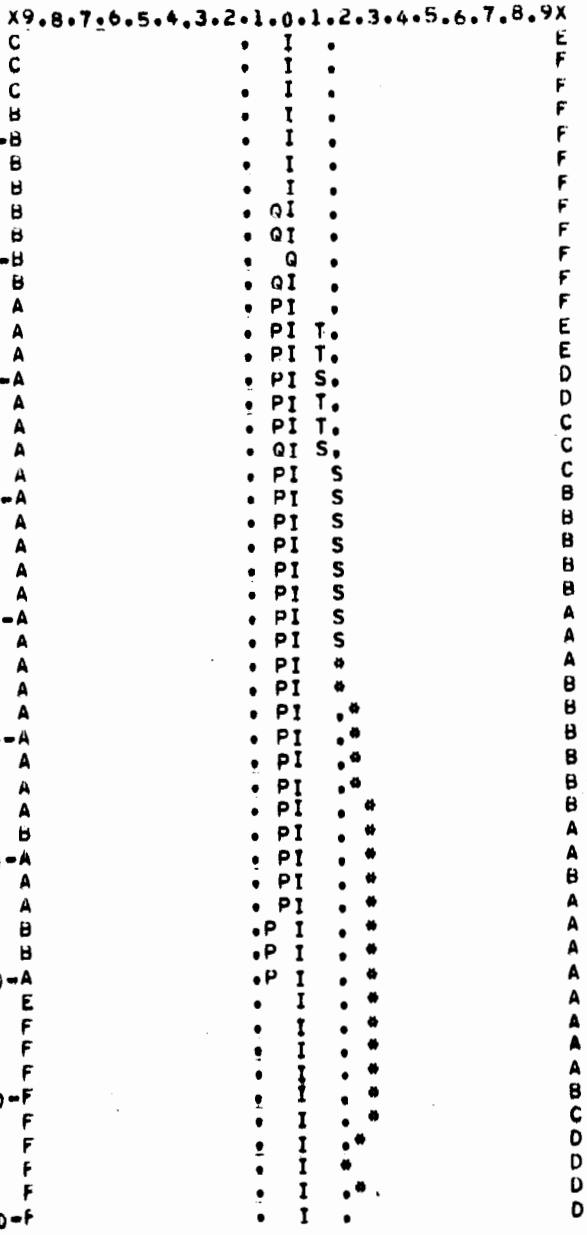

FIGURE 3.1b TRACKING ESTIMATOR OUTPUT IN CALM AIR USING OUTER BASE-LINE SENSORS WITH BAC TRIDENT VORTICES

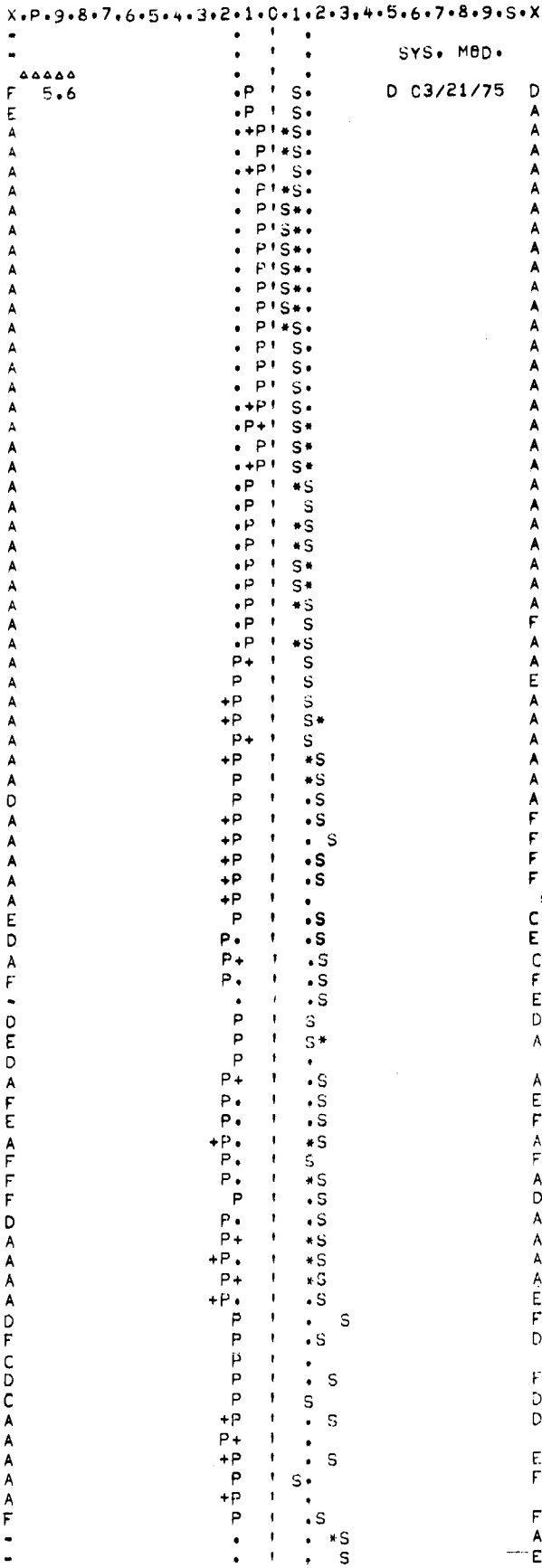

FIGURE 3.2a TSC PROGRAM OUTPUT IN CALM AIR USING INNER BASELINE SENSORS WITH BAC TRIDENT VORTICES

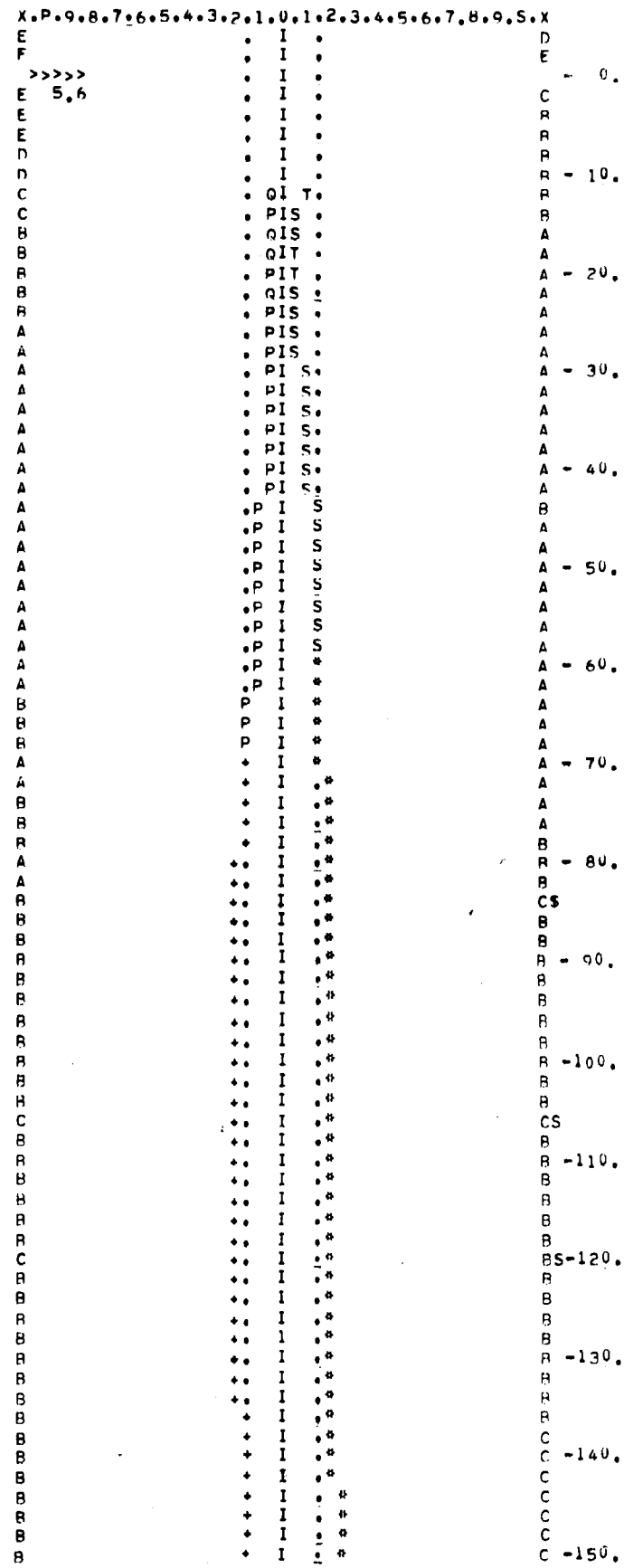

FIGURE 3.2b TRACKING ESTIMATOR OUTPUT IN CALM AIR USING INNER BASELINE SENSORS WITH BAC TRIDENT VORTICES

```
     X9.8.7.6.5.4.3.2.1.0.1.2.3.4.5.6.7.8.9X
     F              P  .  !  .     S        B
     -                 .  !  .     S        C
     D                 .P !  .
     B                 .P !  .        S     D
 10.-A                 .P !  .        S     A
     A                 .+P! S.              F
     A                 . P! S.              B
     A                 . P! S.              B
     A                 . P!  .  S           F
 20.-D                 . P! S.              A
     A                 . P! S.              A
     A                 . P! S.              A
     A                 . P! S.              A
     A                 . P! S.              A
 30.-A                 . P! S.              A
     A                 . P! S.              AS
     A                 . P! S.              A
     A                 . P! S.              A
     A                 . P! S.              A
 40.-A                 . P! S.              A
     A                 . P! S*              A
     A                 . P! *S              A
     A                 . P! S*              A
     A                 . P! *S              A
 50.-A                 . P!  S              A
     A                 .+P!  S              A
     A                 .+P!  S              A
     A                 .+P!  S              A
     A                 .P+!  S              A
 60.-A                 .P !  S              A
     A                 .P !  S              A
     A                 .P !  S              A
     A                 .P !  S*             A
     A                 .P !  S*             A
 70.-A                 .P !  S*             A
     A                 .P !  S*             A
     A                 P+ !  S*             A
     A                 +P !  *S             A
     A                 .P !  .S             A
 80.-A                 .P !  .S*            A
     A                 .P !  . S            B
     A                 .P !  . S            C
     A                 .P !  . S            E
     A                 .P !  . S            A
 90.-A                 .P !  . S            A
     A                 .P !  . S            A
     A                 .P !  . S            D
     A                 .+P!  . S            F
     A                 .P+!  . S            A
100.-A                 .P !  . S            F
     D                 .P !  . S*           A
     -                 .  !  . S            A
     A                 .P !  . S            A
     A                 .P !  . S            E
110.-A                 .P !  . S            A
     A                 .P+!  . S            A
     -                 .  !  . S            A
     D                 .P !  . S            B
     A                 .P !  . S            F
120.-A                 +P !  . S            A
     A                 .P !  . S            F
     A                 +P !  . S            A
     A                 P+ !  .  S           F
     A                 .P !  . S            E
130.-F                 SP !  .              F
```

FIGURE 3.3a TSC PROGRAM OUTPUT IN CALM AIR USING OUTER BASELINE SENSORS WITH DOUGLAS DC-9 VORTICES

```
     X9.8.7.6.5.4.3.2.1.0.1.2.3.4.5.6.7.8.9X
     E                 .  I  .              F
     E                 .  I  .              F
     E                 .  I  .              F
     E                 .  I  .              E
 10-D                  .  I  .              E
     D                 . QI  .              E
     C                 . PI T.              D
     C                 . PI S.              D
     C                 . PI  .              C
 20-C                  . PI T.              C
     B                 . QI S.              C
     B                 . PI T.              B
     B                 . PI S.              B
     B                 . PI T.              B
 30-A                  . PI T.              B
     C                 . PI S.              CS
     B                 . PI T.              B
     B                 . QI S.              B
     B                 . QI S.              B
 40-B                  . PI S.              B
     A                 . PI S.              B
     A                 . PI S.              B
     A                 . PI S.              A
     A                 . PI  S              A
 50-A                  . PI  S              A
     A                 . PI  S              A
     A                 . PI  S              A
     A                 . PI  S              A
     A                 . PI  S              A
 60-A                  .P I  S              A
     A                 .P I  S              A
     A                 .P I  S              A
     A                 .P I  S              A
     A                 .P I  *              A
 70-A                  .P I  *              A
     A                 .P I  *              A
     A                 .P I  *              A
     A                 .P I  *              A
     A                 .P I  .*             A
 80-A                  .P I  .*             A
     A                 .P I  .*             B
     A                 .P I  . *            B
     A                 .P I  . *            B
     A                 .P I  . *            B
 90-A                  .P I  . *            A
     A                 .P I  . *            A
     A                 .P I  . *            B
     A                 .P I  . *            C
     A                 .P I  . *            B
100-A                  .P I  .*             C
     A                 .P I  .*             C
     B                 .P I  . *            C
     A                 .P I  . *            C
     A                 .P I  .*             C
110-A                  .P I  . *            C
     A                 .P I  . *            B
     E                 .  I  . *            B
     E                 .  I  . *            C
     E                 .  I  .*             D
120-D                  .  I  .*             C
     D                 .  I  .*             C
     C                 .  I  .              C
     C                 .  I  .              C
     C                 .  I  .              C
130-D                  .  I  .              E
```

FIGURE 3.3b TRACKING ESTIMATOR OUTPUT IN CALM AIR USING OUTER BASELINE SENSORS WITH DOUGLAS DC-9 VORTICES

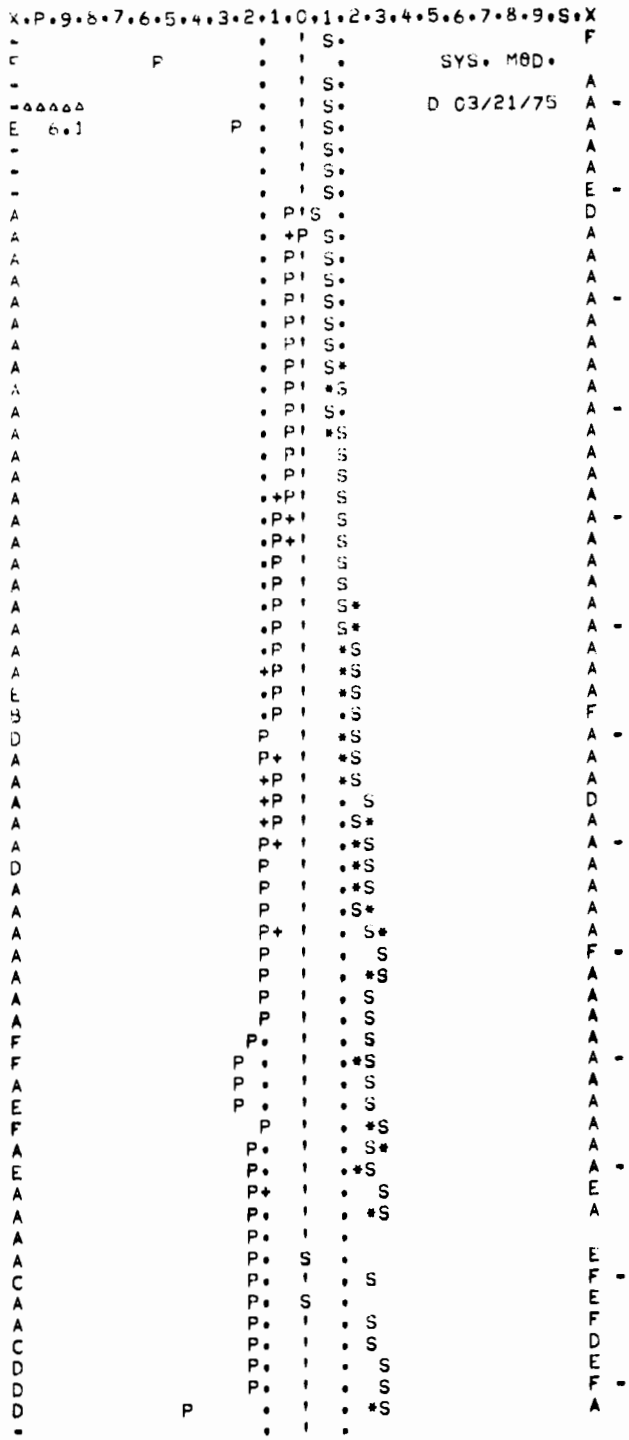

FIGURE 3.4a TSC PROGRAM OUTPUT IN CALM AIR USING INNER BASELINE SENSORS WITH DOUGLAS DC-9 VORTICES

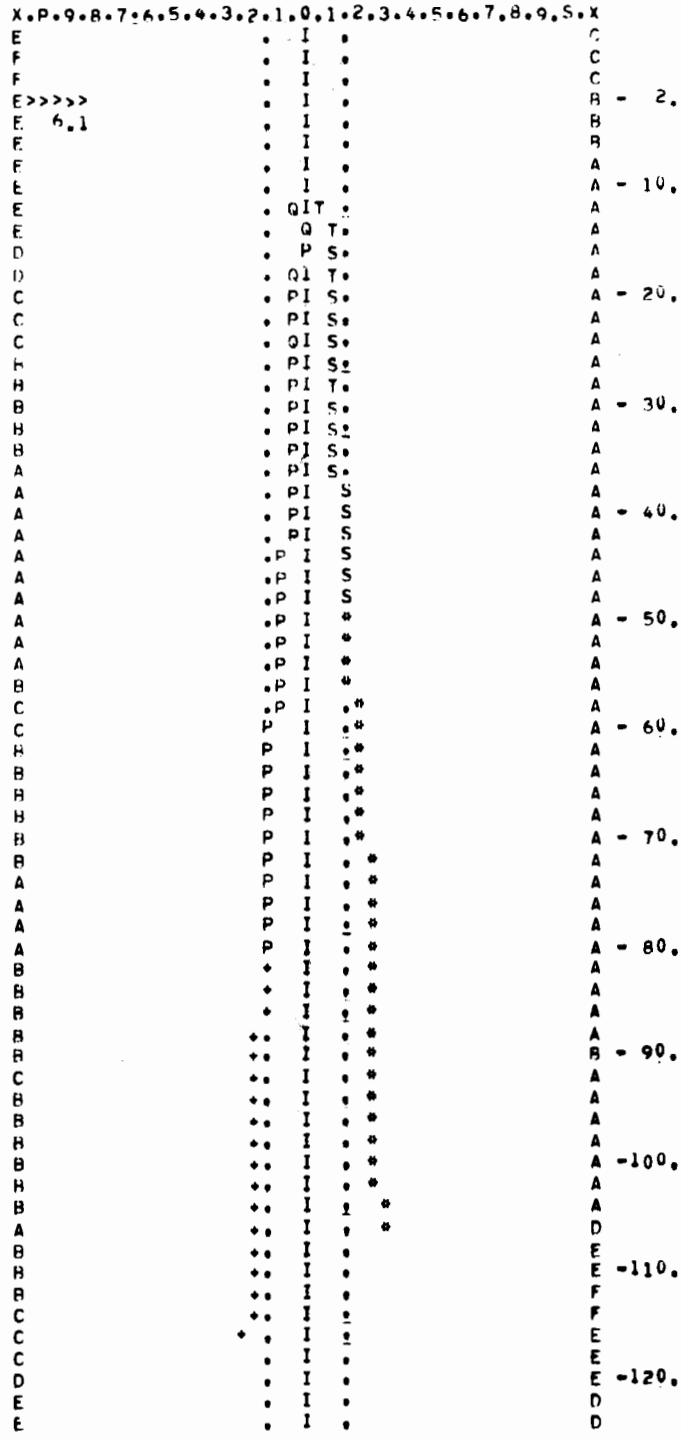

FIGURE 3.4b TRACKING ESTIMATOR OUTPUT IN CALM AIR USING INNER BASELINE SENSORS WITH DOUGLAS DC-9 VORTICES

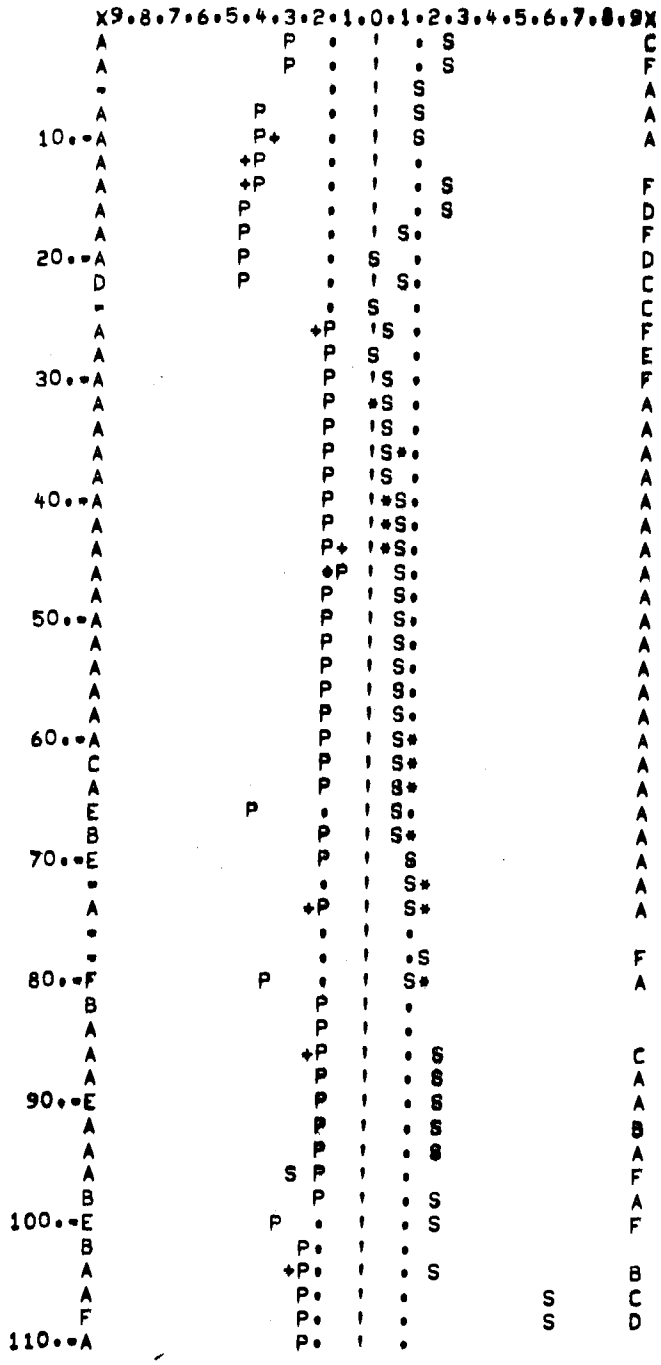

FIGURE 3.5a TSC PROGRAM OUTPUT IN CALM AIR USING OUTER BASELINE SENSORS WITH BOEING 737 VORTICES

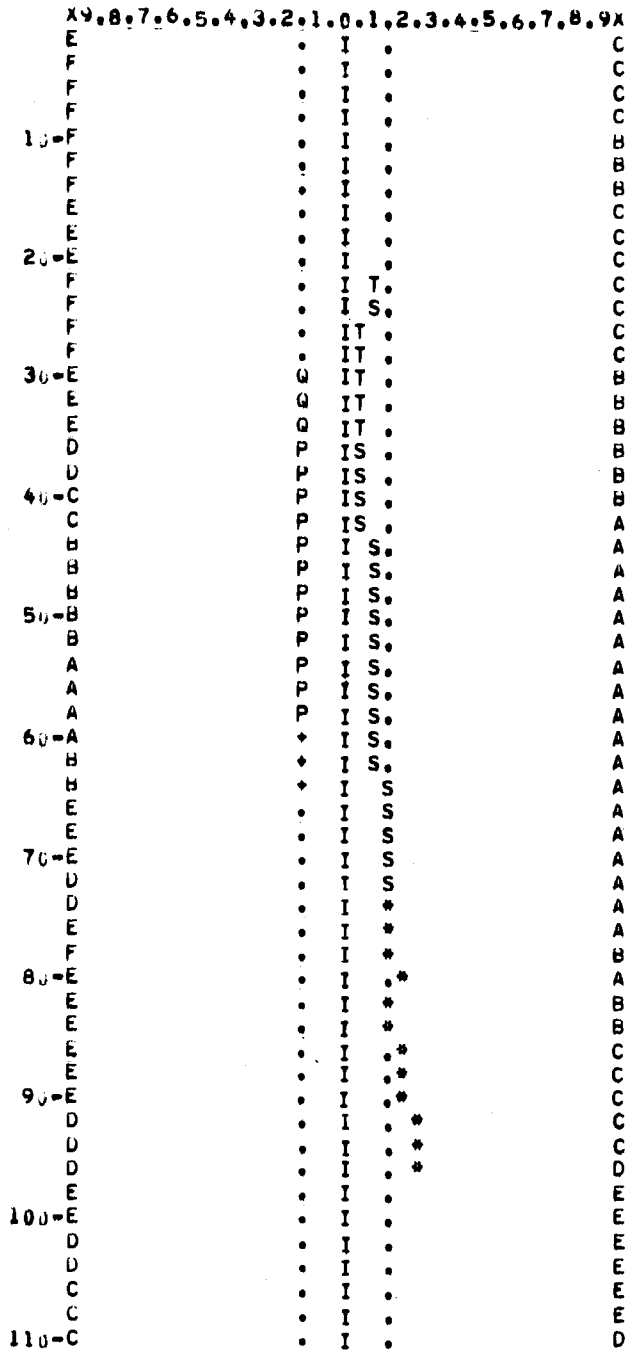

FIGURE 3.5b TRACKING ESTIMATOR OUTPUT IN CALM AIR USING OUTER BASELINE SENSORS WITH BOEING 737 VORTICES

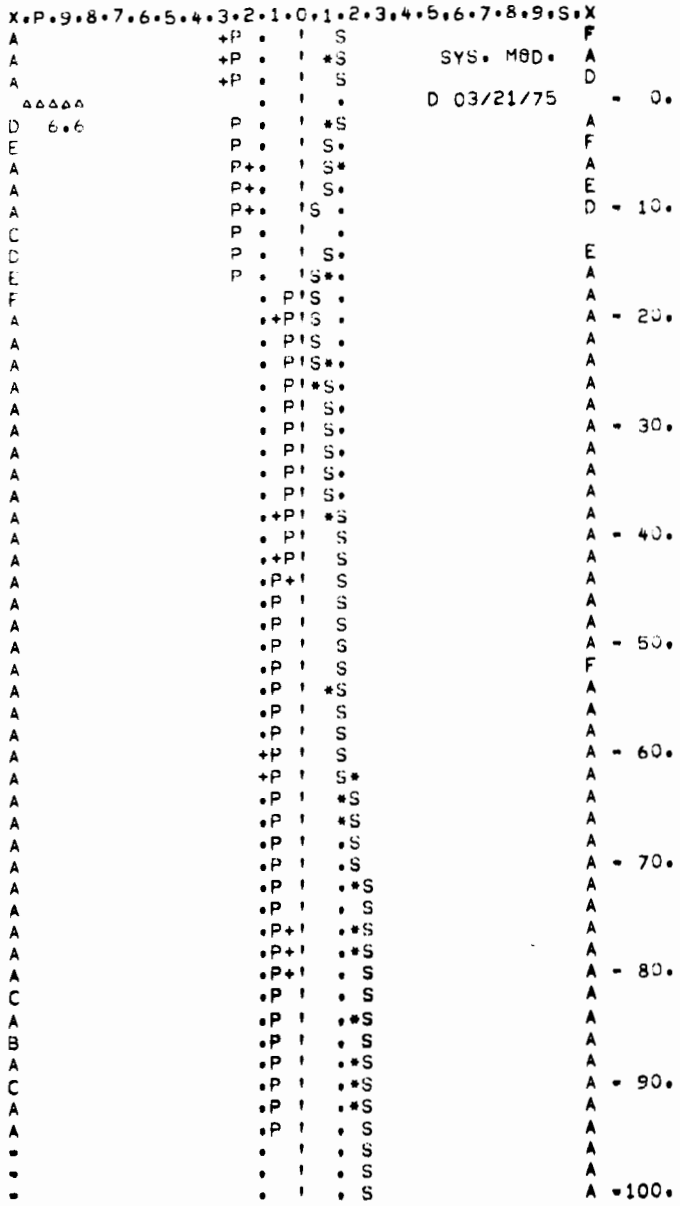

FIGURE 3.6a TSC PROGRAM OUTPUT IN CALM AIR USING INNER BASELINE SENSORS WITH BOEING 737 VORTICES

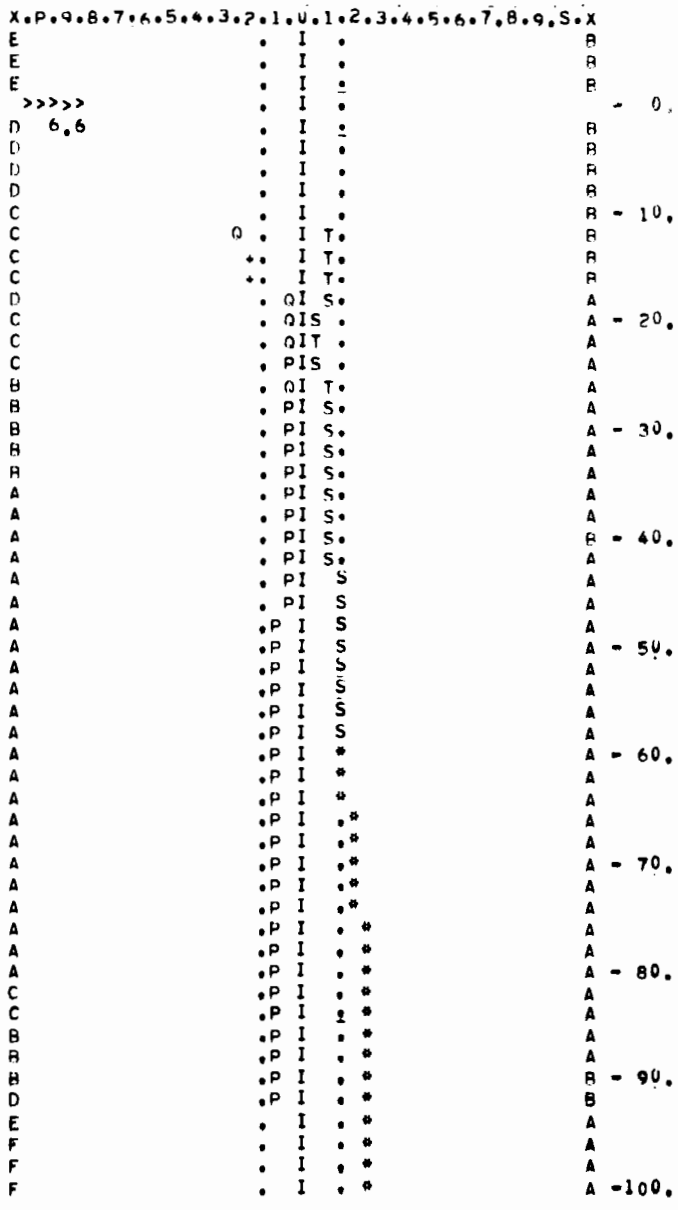

FIGURE 3.6b TRACKING ESTIMATOR OUTPUT IN CALM AIR USING INNER BASELINE SENSORS WITH BOEING 737 VORTICES

seconds due to poor tracking quality. Tracking quality, as described in Section 2.7, is printed in the column running down the left-hand side of the figure for the port-vortex estimator, and down the right-hand side for the starboard-vortex estimator. As can be seen, the port-vortex quality falls abruptly from A to E at 82 seconds, precipitating track termination in response to the erratic behavior of the sensor data. In the period from about 20 seconds until 80 seconds the estimates are very good, as indicated by the A and B grades attained in that period. The starboard-vortex track is initialized at 26, 28, 32, and 34 seconds. The track passes beyond the +150 ft boundary at 54 seconds, as evidenced by the change from S to *, in Fig. 3.1b, to indicate starboard-vortex position outside the ±150-ft region. If the port vortex had passed outside the ±150-ft region the P would have changed to + indicating a port vortex positioned outside the ±150-ft region. The starboard-vortex track terminates at 98 seconds when the sensor data become erratic. The starboard-track estimator produces a smooth track with high-quality tracking from 40 seconds to 90 seconds. Track termination is slightly late, as evidenced by the rather abrupt and unrealistic motion of the estimate from 94 to 98 seconds.

The inner baseline data taken for the same period, Tape HM-94 (Case 11), are presented in Fig. 3.2. Figure 3.2a represents the TSC program output, and Fig. 3.2b shows the tracking-estimator output. Performance of the tracking estimator is similar to what was observed in Fig. 3.1. In this case, however, when the tracking data begin to deteriorate after 120 seconds, the estimator tracker is able to continue to track through the bad period and the starboard track is not terminated until 170 seconds. Port-vortex data begin to deteriorate after 140 seconds, and the tracking estimator terminates the port track at about 150 seconds. It should be noted, however, that even though a vortex is reported after 120 seconds, it is likely that its strength is greatly diminished.

Figures 3.3a and 3.3b present data for the outer baseline sensors with a small transport aircraft, in this case a Douglas DC-9. These data are from Tape HM-94 (Case 12). Good sensor data are available until about 110 to 120 seconds, when the tracker estimator terminates the tracks. Tracking quality is quite high over the entire tracking interval.

Figures 3.4a and 3.4b represent the same case but for these figures the data were obtained from the inner baseline sensors. The starboard-vortex track in Fig. 3.4b illustrates the ability of the tracking estimator to filter out sensor errors and produce a smooth estimate in the face of rather erratic sensor data.

Figures 3.5 and 3.6 present tracking data for a Boeing 737 transport. These data are from Tape HM-94 (Case 16). The port track in Fig. 3.5b terminates early in response to erratic sensor data at about 65 seconds, as can be seen in Fig. 3.5a. Comparison of Figs. 3.6a and 3.6b demonstrates the ability of the tracker estimator to lock onto a new vortex, as its effect appears in the sensors, when the remnant of an old vortex still remains in the sensor line, as evidenced by the port-vortex indications in Fig. 3.6a, at -250 ft, up until about 16 seconds.

3.2 VORTEX TRACKING IN STRONG HEADWINDS

In strong headwinds the tracking task is far more difficult than in calm air. There is sizable turbulence which in turn produces signals in the sensor outputs which mask the vortex tracks. Furthermore, the vortices dissipate quickly and the process of track termination is more critical. On the other hand, the signal-to-noise ratios are generally low, and the tracking estimator must be made rather sensitive to detect marginal signals so spurious signals must not be identified as vortex tracks. Hence, a fine balance must be struck between sensitivity and the ability to reject spurious signals.

Figures 3.7a and 3.7b present outer baseline tracking data from Heathrow Tape HM-95 (Case 8) with vortices produced by a Boeing 727 aircraft. Figure 3.7a, which is the output from the TSC program, serves to indicate the poor quality of the sensor tracking data, due primarily to headwinds of about 25 ft/sec. No coherent starboard vortex track is evident, and only the trace of a port vortex track appears on Figure 3.7a. Figure 3.7b presents the output from the vortex-tracking estimator. No starboard track is reported, but the estimator is able to track the port vortex from about 34 seconds to 60 seconds. Figures 3.8a and 3.8b present the TSC program outputs and tracking-estimator outputs, respectively, using the inner baseline sensor data for the same case. Here the sensor data are better, and both port and starboard vortices are reported by the tracking estimator. The vortices are acquired promptly at about 15 seconds and are terminated appropriately at about 34 seconds. Tracking quality is generally marginal, as evidenced by the grades received while tracking.

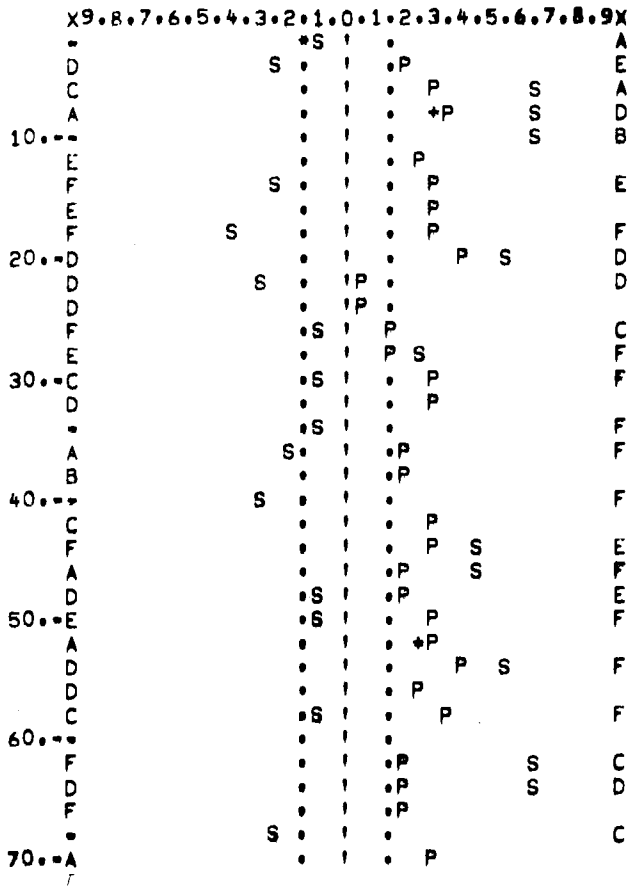

FIGURE 3.7a TSC PROGRAM OUTPUT IN STRONG HEADWINDS USING OUTER BASELINE SENSORS WITH BOEING 727 VORTICES

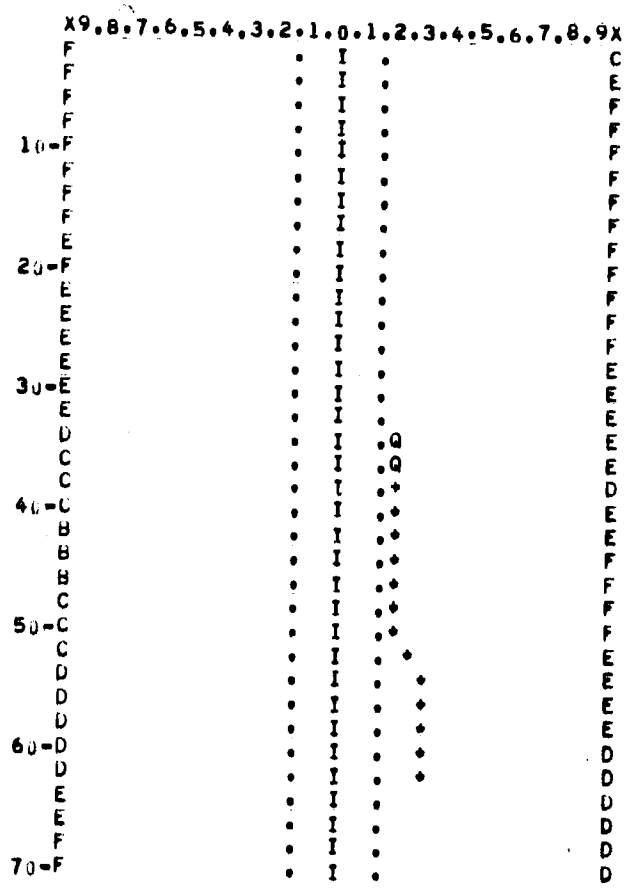

FIGURE 3.7b TRACKING ESTIMATOR OUTPUT IN STRONG HEADWINDS USING OUTER BASELINE SENSORS WITH BOEING 727 VORTICES

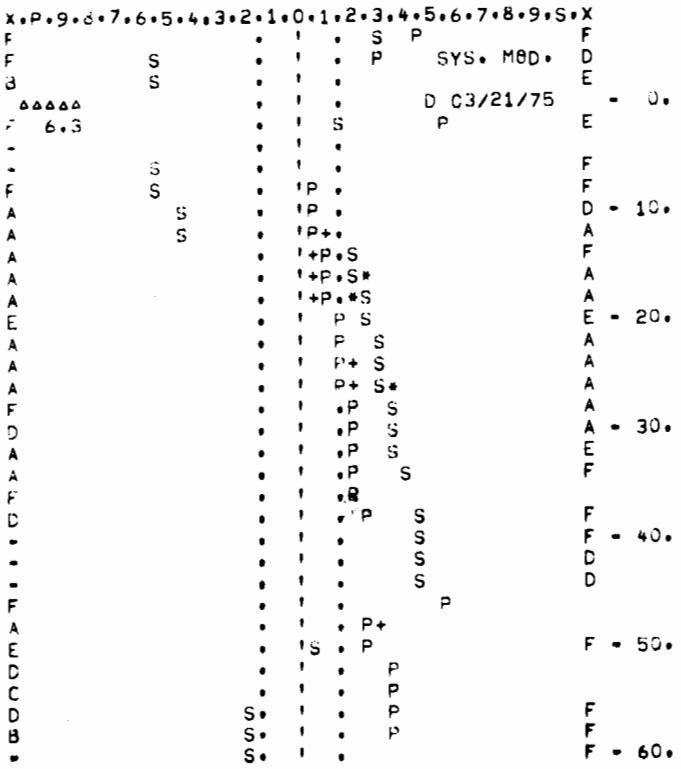

FIGURE 3.8a TSC PROGRAM OUTPUT IN STRONG HEADWINDS USING INNER BASELINE SENSORS WITH BOEING 727 VORTICES

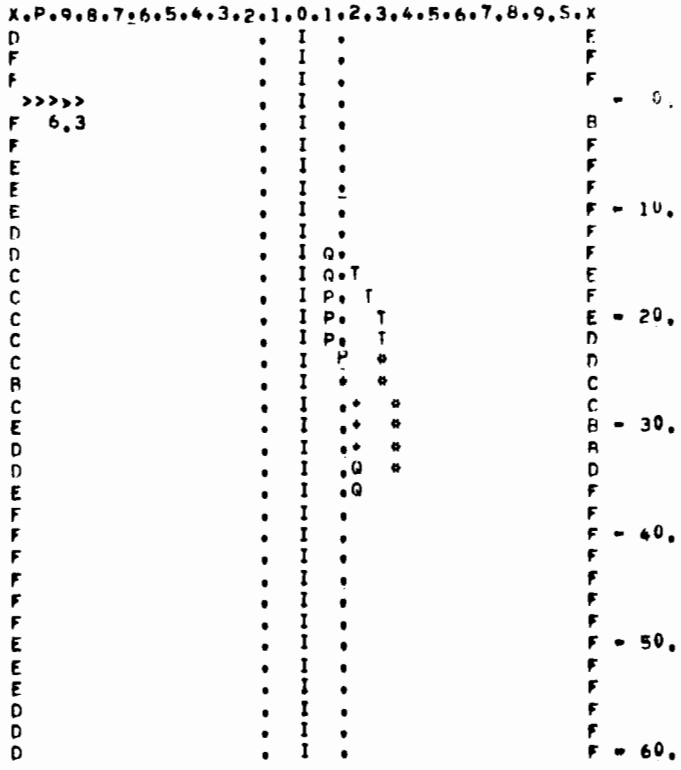

FIGURE 3.8b TRACKING ESTIMATOR OUTPUT IN STRONG HEADWINDS USING INNER BASELINE SENSORS WITH BOEING 727 VORTICES

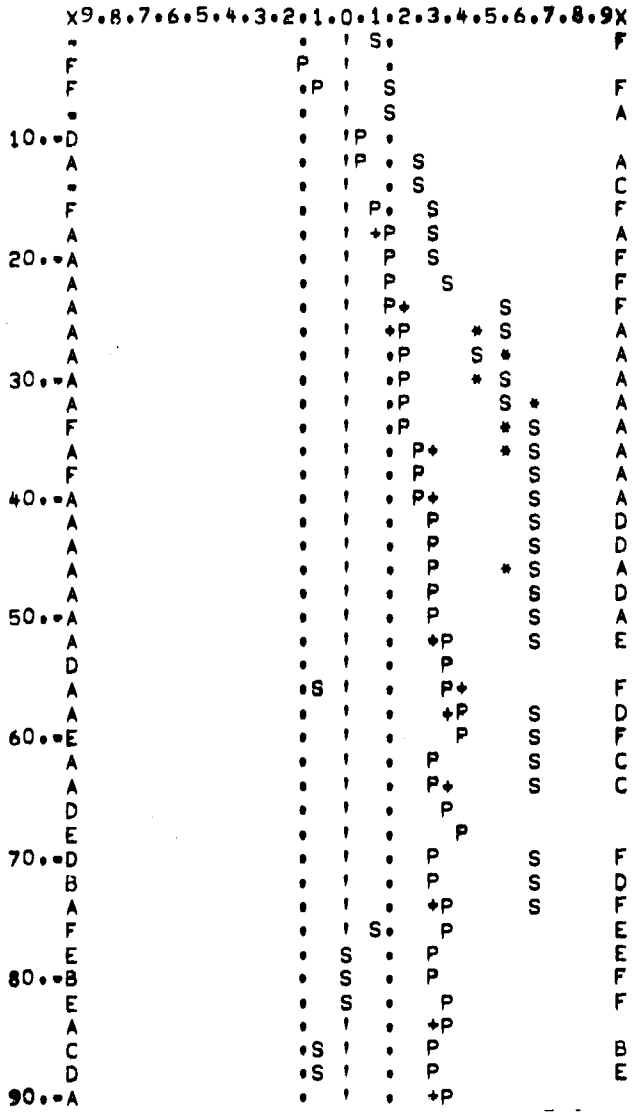

FIGURE 3.9a TSC PROGRAM OUTPUT IN STRONG HEADWINDS USING OUTER BASELINE SENSORS WITH BOEING 747 VORTICES

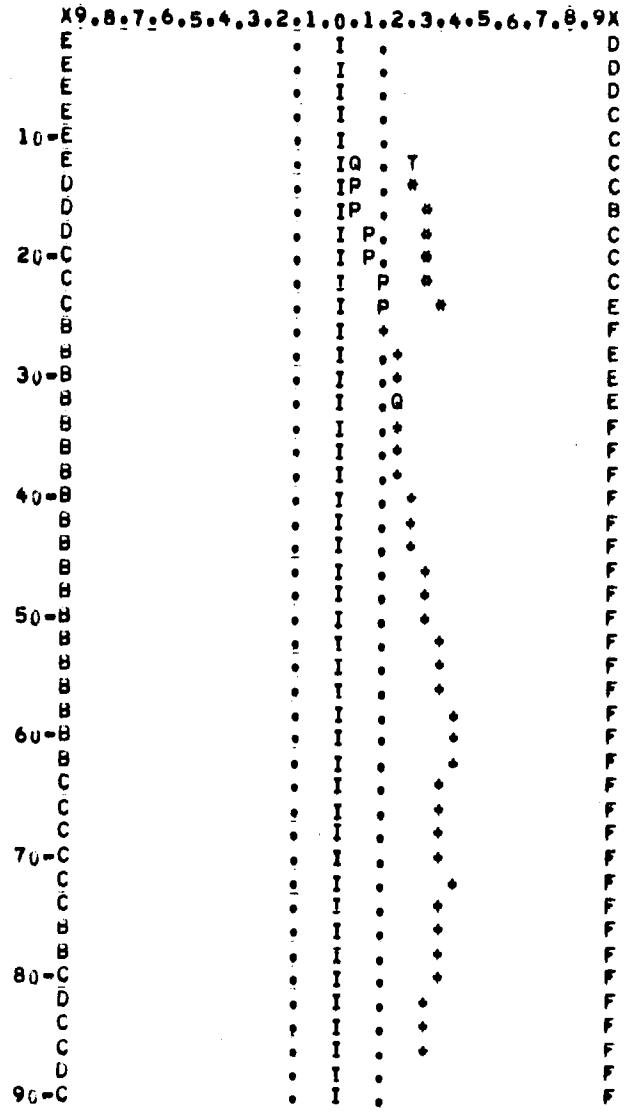

FIGURE 3.9b TRACKING ESTIMATOR OUTPUT IN STRONG HEADWINDS USING OUTER BASELINE SENSORS WITH BOEING 747 VORTICES

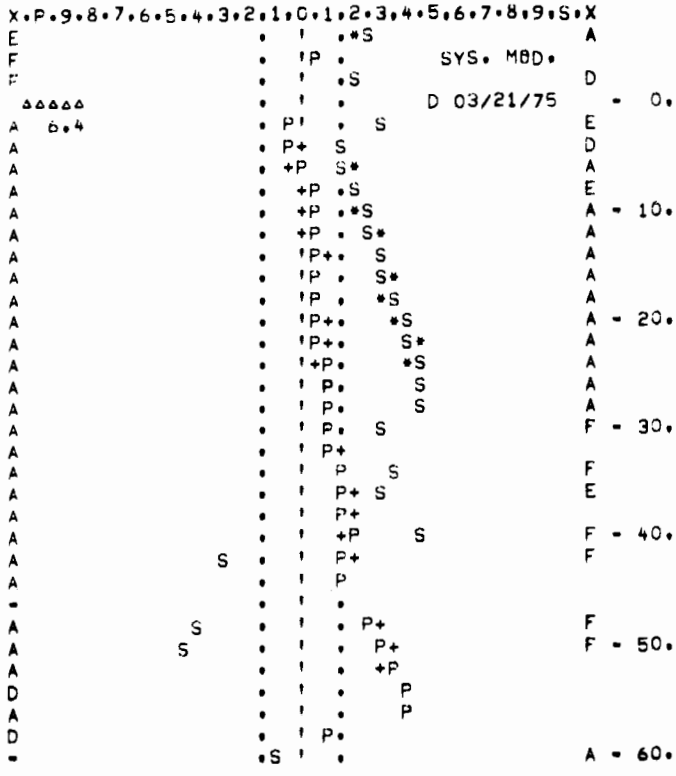

FIGURE 3.10a TSC PROGRAM OUTPUT IN STRONG HEADWINDS USING INNER BASELINE SENSORS WITH BOEING 747 VORTICES

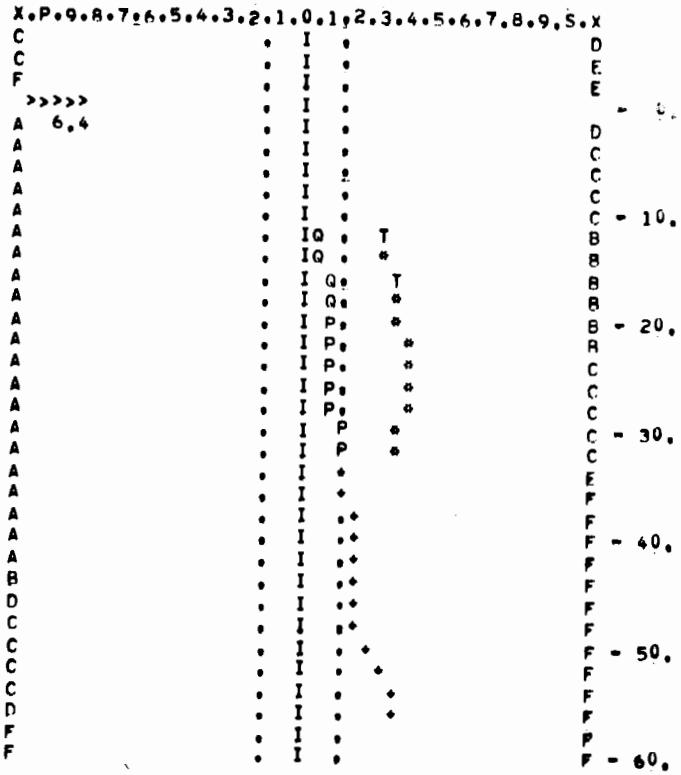

FIGURE 3.10b TRACKING ESTIMATOR OUTPUT IN STRONG HEADWINDS USING INNER BASELINE SENSORS WITH BOEING 747 VORTICES

Figures 3.9 and 3.10 are again a high-headwind case from Tape HM-95 (Case 6); with a large aircraft, in this case a Boeing 747. Figures 3.9a and 3.9b represent the outer baseline sensor data, processed through the TSC program and the tracking estimator, respectively. As seen in Fig. 3.9a, the starboard vortex passes outside the sensor line in about 40 seconds. After that time the sensor at +650 ft. continues to have the highest output, resulting in the column of starboard indications at +650 ft., from 40 seconds until 74 seconds. The estimator tracker rejects this spurious signal by terminating the starboard track, due to poor tracking quality, at 24 seconds. The termination is slightly premature in that the track might have been prolonged until about 34 seconds. The port-vortex track continues until 86 seconds, at which point the signal-to-noise ratio falls below 2 and the track is terminated.

Figures 3.10a and 3.10b reveal the tracking results for the inner baseline sensor data for the same case (HM-95, Case 6). Signals are strong enough, with this large aircraft, to produce excellent tracking of the port vortex and reasonably good tracking of the starboard vortex. Erratic sensor outputs cause loss of tracking quality and termination of both vortex tracks.

3.3 VORTEX TRACKING IN STRONG CROSSWINDS

As was the case with strong headwinds, strong crosswinds cause difficulty in vortex tracking. The two most important factors affecting tracking performance are turbulence and the fact that the wind may displace the vortices by hundreds of feet from the runway centerline before they begin to produce useful sensor data.

Figures 3.11a and 3.11b are the outputs from the TSC program and the tracking estimator, produced from outer baseline sensor data using Tape HM-62 (Case 11). A light transport aircraft, in this case a Caravelle, produced the vortices. Sensor outputs are generally erratic, as can be seen in Fig. 3.11a, and, hence, no coherent vortex tracks are reported by the tracking estimator.

Figures 3.12a and 3.12b show the results of processing inner baseline data. In this case the starboard data are quite erratic, but a port-vortex track is discernable in Fig. 3.12a from 12 to 40 seconds. This signal is tracked by the tracking estimator from 20 seconds until 32 seconds, at which point the track is terminated due to poor tracking quality.

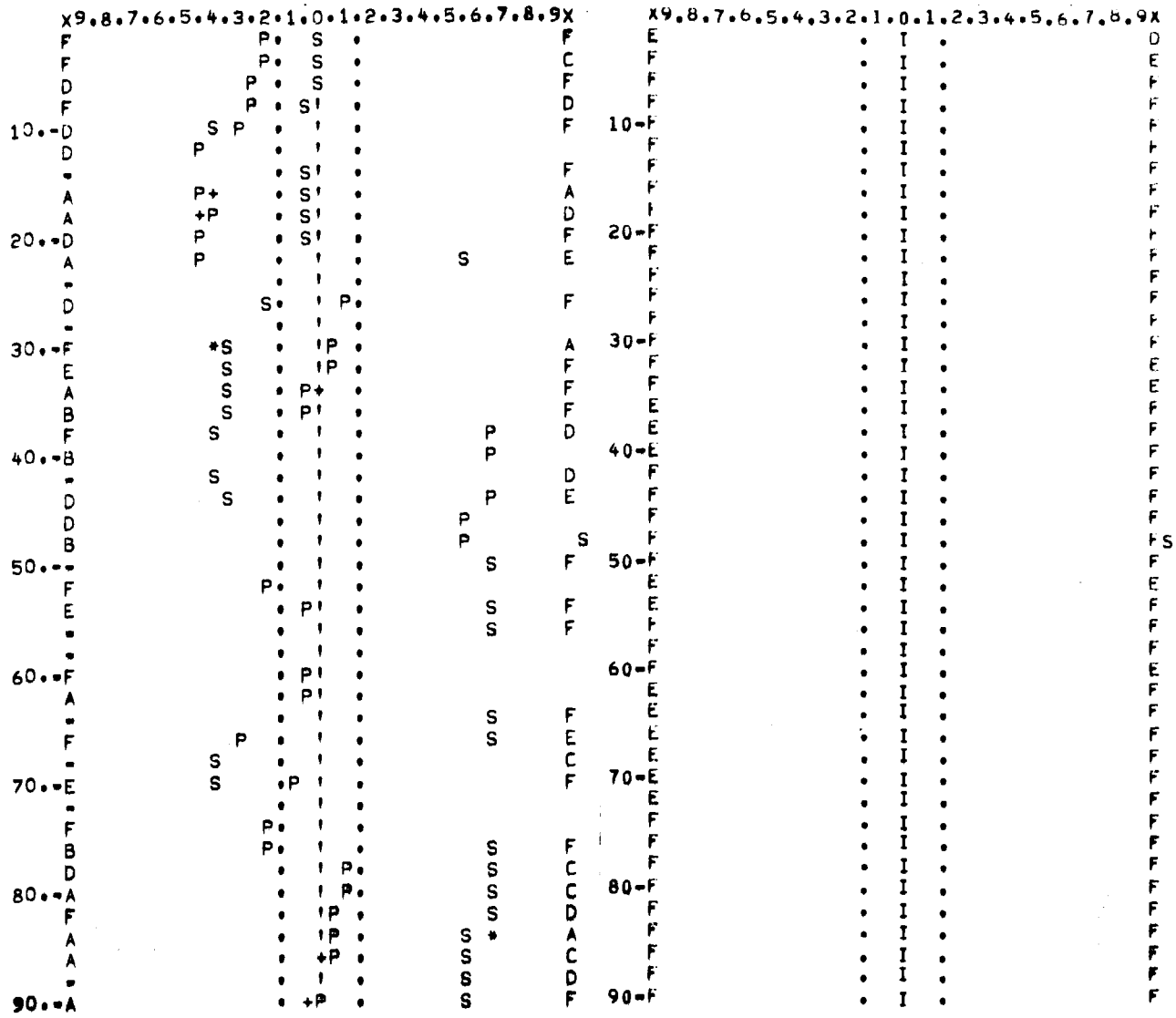

FIGURE 3.11a TSC PROGRAM OUTPUT IN STRONG CROSSWINDS USING OUTER BASELINE SENSORS WITH CARAVELLE VORTICES

FIGURE 3.11b TRACKING ESTIMATOR OUTPUT IN STRONG CROSSWINDS USING OUTER BASELINE SENSORS WITH CARAVELLE VORTICES

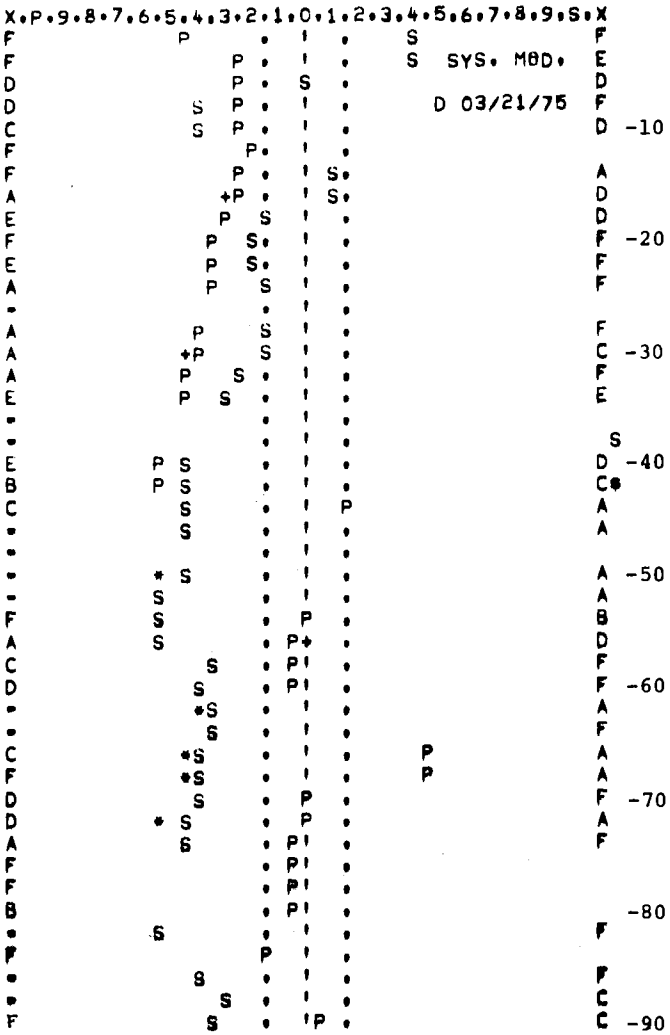

FIGURE 3.12a TSC PROGRAM OUTPUT IN STRONG CROSSWINDS USING INNER BASELINE SENSORS WITH CARAVELLE VORTICES

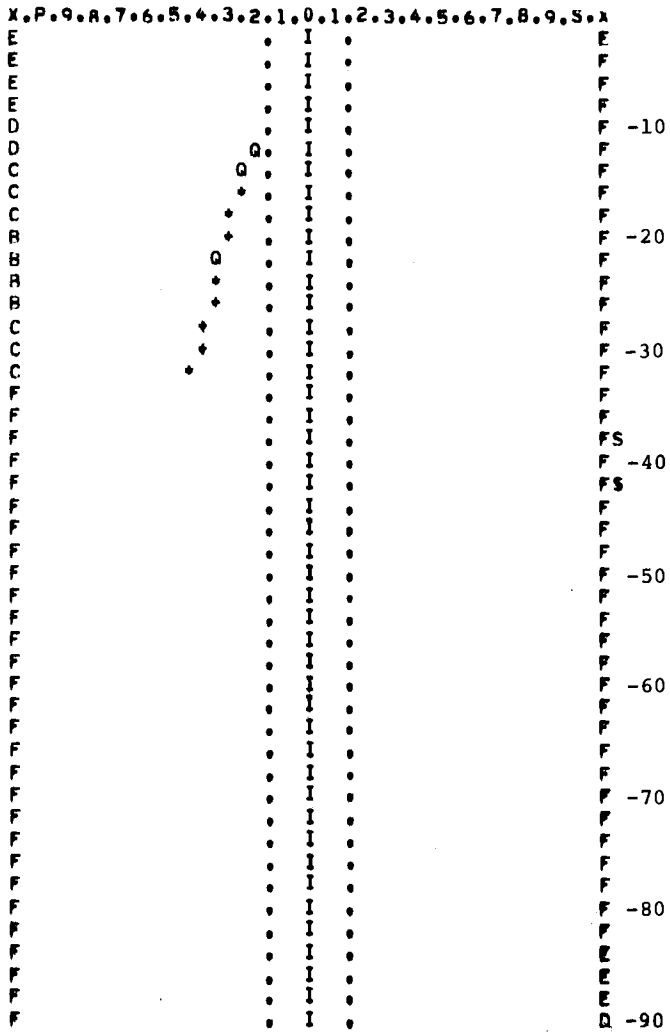

FIGURE 3.12b TRACKING ESTIMATOR OUTPUT IN STRONG CROSSWINDS USING OUTER BASELINE SENSORS WITH CARAVELLE VORTICES

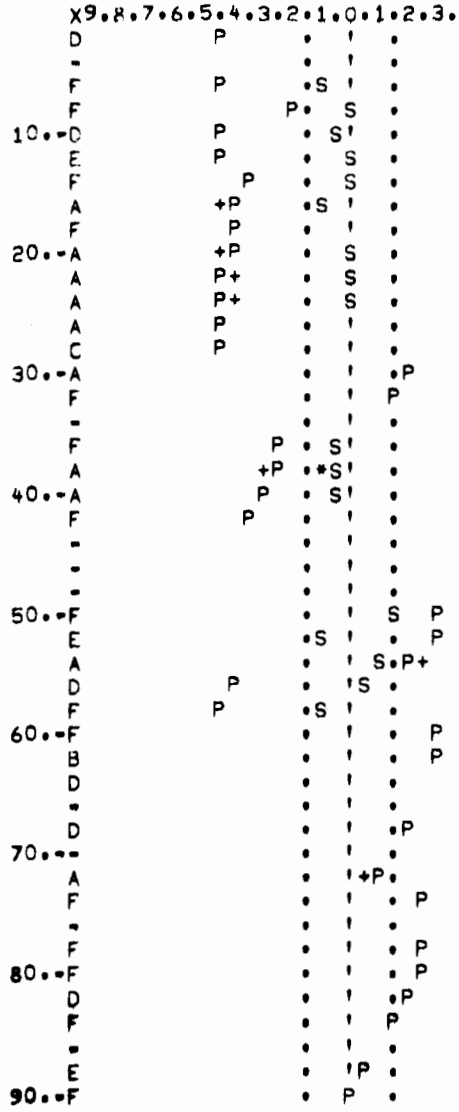

FIGURE 3.13a TSC PROGRAM OUTPUT IN STRONG CROSSWINDS USING OUTER BASELINE SENSORS WITH BOEING 737 VORTICES

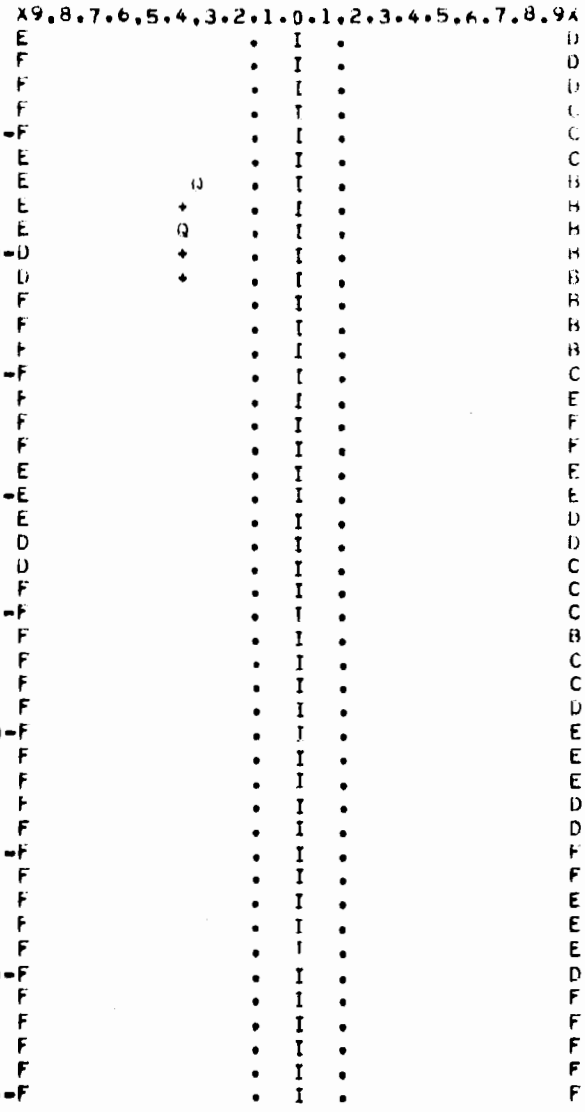

FIGURE 3.13b TRACKING ESTIMATOR OUTPUT IN STRONG CROSSWINDS USING OUTER BASELINE SENSORS WITH BOEING 737 VORTICES

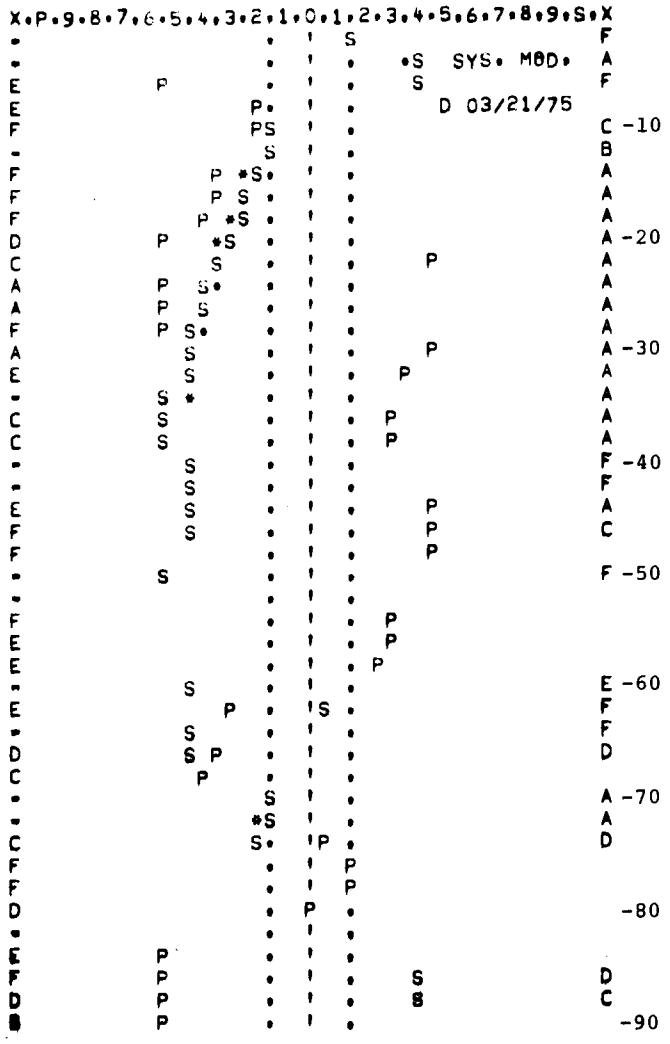

FIGURE 3.14a TSC PROGRAM OUTPUT IN STRONG CROSSWINDS USING INNER BASELINE SENSORS WITH BOEING 737 VORTICES

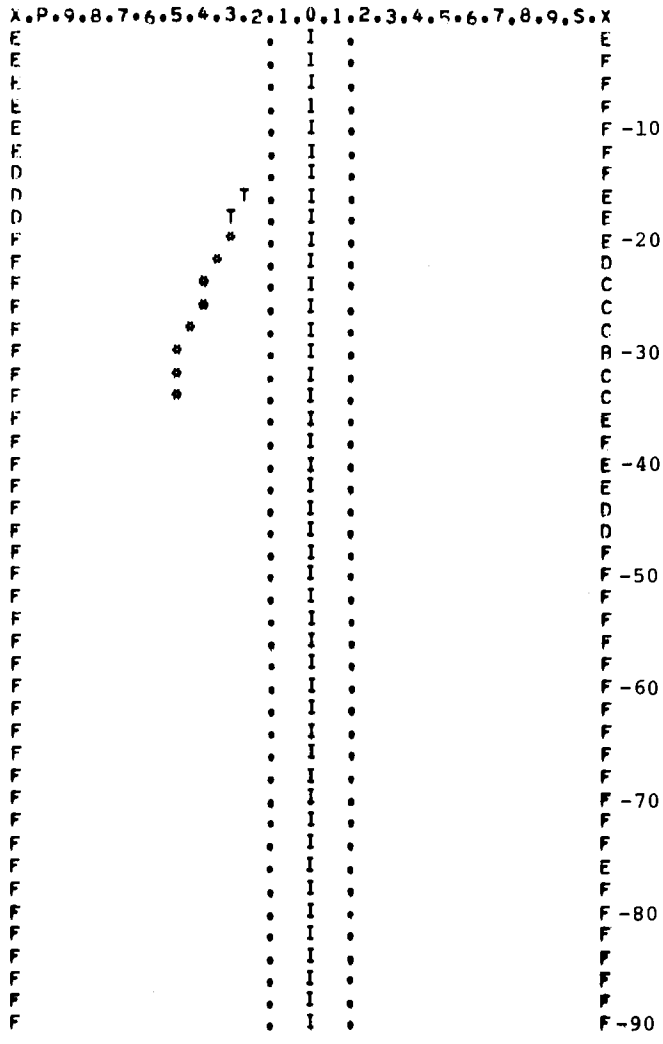

FIGURE 3.14b TRACKING ESTIMATOR OUTPUT STRONG CROSSWINDS USING INNER BASELINE SENSORS WITH BOEING 737 VORTICES

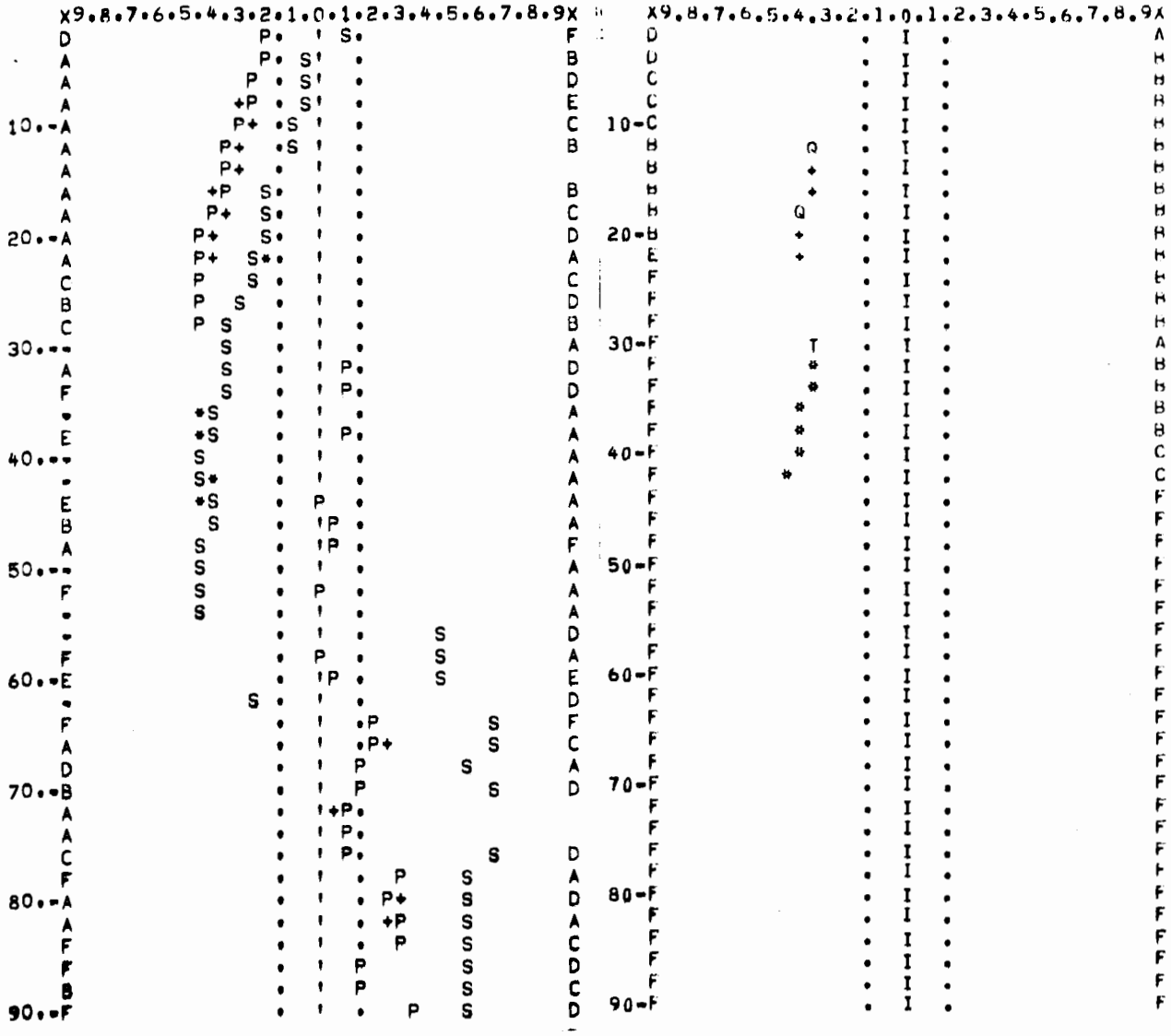

FIGURE 3.15a TSC PROGRAM OUTPUT IN STRONG CROSSWINDS USING OUTER BASELINE SENSORS WITH A-300 AIRBUS VORTICES

FIGURE 3.15b TRACKING ESTIMATOR OUTPUT IN STRONG CROSSWINDS USING OUTER BASELINE SENSORS WITH A-300 AIRBUS VORTICES

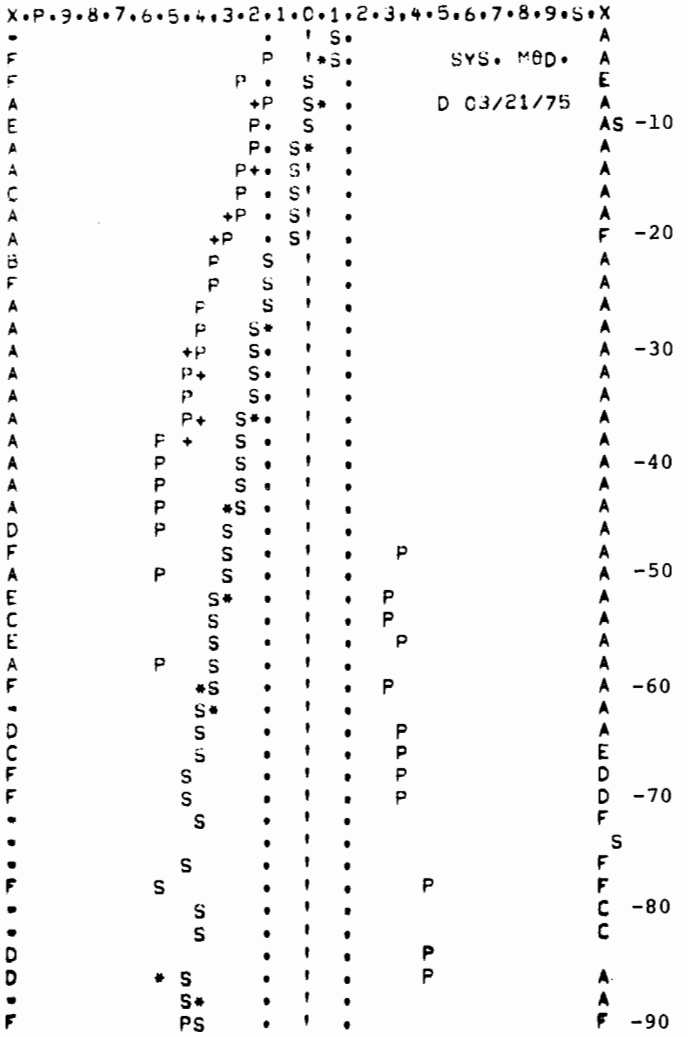

FIGURE 3.16a TSC PROGRAM OUTPUT IN STRONG CROSSWINDS USING INNER BASE-LINE SENSORS WITH A-300 AIRBUS VORTICES

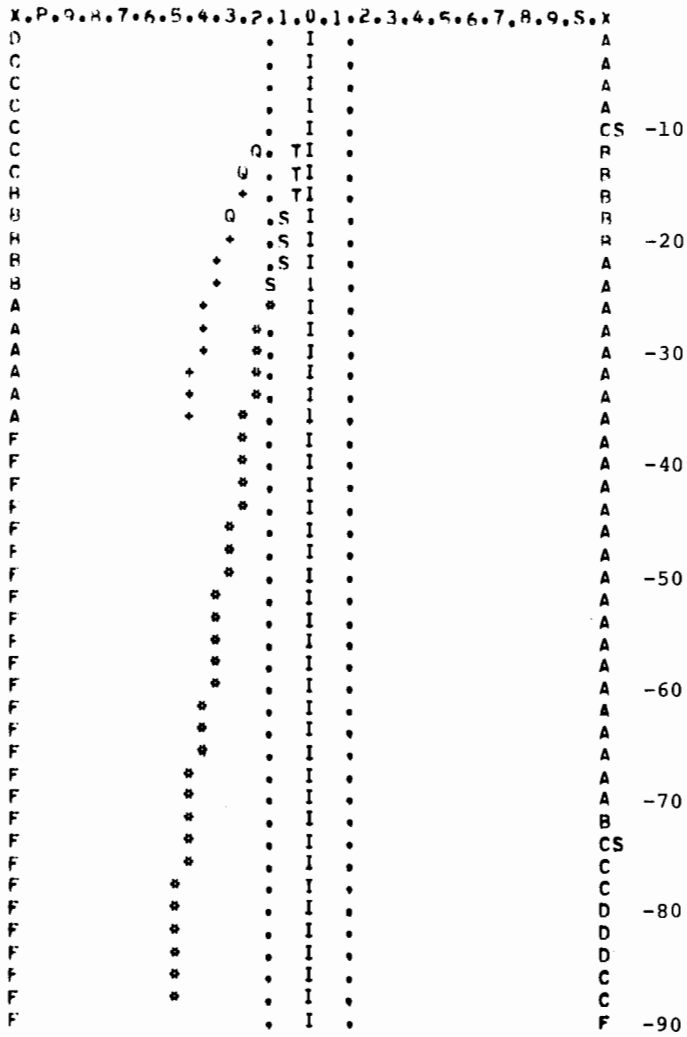

FIGURE 3.16b TRACKING ESTIMATOR OUTPUT IN STRONG CROSSWINDS USING INNER BASELINE SENSORS WITH A-300 AIRBUS VORTICES

Figures 3.13a and 3.13b illustrate tracking under similar conditions for a Boeing 737. The data are the outer baseline sensor outputs from Tape HM-62 (Case 3). Erratic sensor outputs prevent effective tracking of the starboard vortex; however, the trace of a port-vortex track can be seen in Fig. 3.13a and the tracking estimator barely catches the track in Fig. 3.13b.

Figures 3.14a and 3.14b show the inner baseline results for the same case. The port vortex does not produce a sufficiently high signal-to-noise ratio for tracking, but the starboard vortex is tracked from 16 seconds to 34 seconds. Tracking quality is relatively poor due to erratic sensor data.

Figures 3.15a and 3.15b show results for an A-300 Airbus. The data were obtained from the outer baseline sensors with Tape HM-62 (Case 1). The tracking estimator produces only short tracks. The delay in initialization of the starboard track is the result of a low signal-to-noise ratio until 30 seconds.

Finally, Figs. 3.16a and 3.16b show results for the same case using data from the inner baseline sensors. Large signal-to-noise ratios produce high-quality tracking over most of the tracking period. Abrupt loss of quality is due to passage of the vortices beyond the sensor line.

3.4 VORTEX TRACKING RESULTS SUMMARY

The results presented are typical of many vortex tracks produced with real data from the Heathrow tapes. Typically the tracking estimator, in its current configuration, is conservative in the sense that vortex tracks are initiated somewhat later and terminated somewhat earlier than might be expected from performing visual pattern recognition on the raw data. This type of performance was purposely designed into the system, as a means of preventing the tracker from reporting false vortices in response to turbulence, gusts, or other error sources. The tracker is quite robust, performing well over a wide range of atmospheric conditions and aircraft types, and with data from two separate sensor lines. No external data on aircraft type are required by the tracker and no meteorological data, other than the ground-wind sensor data, are used. In calm air the tracking errors are generally of the order of 25 feet (rms). In turbulent conditions these errors can range up to 150 feet (rms), depending upon the severity of the turbulence and the strength of the vortices.

Experiments were also run with sensors removed from the data, thereby simulating such loss of information as would occur when sensors have failed and have been taken off line. Removal of one sensor has almost no effect on the tracking. Removal of two adjacent sensors introduces some inaccuracy,but the estimator is able to maintain the track across the missing sensors. The loss of three adjacent sensors usually causes difficulty when vortices approach the region normally covered by the three sensors. Hence, a substantial loss of information can be sustained before the estimator becomes ineffective.

The results presented above pertain solely to the performance of a tracking algorithm which systematically analyzes sensor data. It would be a gross error to attempt to evaluate the hazard potential to following aircraft solely from these results. Vortex strength, altitude, and the location of the following aircraft with respect to the vortices cannot be obtained from this algorithm; these parameters being the primary elements in evaluating hazard. The indication of vortices persisting for a long period of time is purely the consequence of the algorithm's ability to process very low-level signals on calm days.

4. SENSOR-FAILURE IDENTIFICATION

The ground-wind anemometers and their associated electronics are subject to occasional failures. Typical failure modes include: physical damage to anemometers, physical misalignment of anemometers, bearing wear, loss of power, 60-cycle interference, scale factor errors, bias shifts, excessive noise in output signals, and many other possible difficulties.

Although there are many failure modes, the resulting effects on sensor output can be categorized in terms of a few general types of failure phenomena. For example, physical damage, misalignment, loss of power, and scale-factor error often manifest themselves primarily as biases. Similarly, bearing failure and 60-cycle interference appear as noise in the output. Hence, the bias shift and excessive noise effectively describe a wide range of failures.

The erroneous signals produced by failures are processed as input data by the vortex tracking estimator. Depending upon the severity of a failure, the resulting effect on tracking performance can range from a slight reduction in tracking accuracy to complete destruction of tracking capability. In order to protect the vortex tracking estimator from ingesting bad data, a sensor failure detection and identification program was developed. This program effectively compares the sensor outputs with each other, utilizing the redundancy inherently available in multiple sensors to find failures. The program looks specifically for bias failures and random noise failures in the sensor output data. When a failure is detected and the bad sensor identified, its output is henceforth ignored and the remaining sensors are used to track vortices. Although there is a resulting loss in information, the tracking estimator has consistently demonstrated its ability to track vortices effectively, even given failures in two adjacent sensors.

4.1 SENSOR BIAS-FAILURE IDENTIFICATION

The sensor bias-failure identification system depends upon comparisons of filtered sensor outputs with each other. No failure identification is attempted while vortices are producing strong signals in the sensors. This is accomplished, in the failure-identification system, by not processing sensor data during the 60 seconds following aircraft detection. The delay effectively gives enough time for the vortices to dissipate to the point where they are no longer a factor in failure detection.

At sample times other than during the 60 second delay after aircraft detection, the output of each sensor is processed through a first-order low-pass filter. There is one filter associated with each sensor, and the filters are all identical, with time constants of 200 seconds. The filters suppress high-frequency noise but pass sensor biases. After all new sensor outputs are processed, the filtered outputs are averaged to obtain the sample mean across the sensor line. Then, the filtered output of each individual sensor is compared with the sample mean, and if deviations of more than five ft/sec are found, the sensor with the largest deviation is designated as failed. The filtered output from that sensor is then eliminated from the sample mean and the mean recalculated. The comparisons and elimination of the sensor with the largest deviation greater than 5 ft/sec are repeated until all deviations are less than 5 ft/sec.

During the 60-second delay allowed for vortex dissipation, no sensor outputs are processed and no failure identification is attempted. To allow long-term analysis of sensor outputs, the filter state variables are simply held constant over the delay period, thereby effectively carrying the past history of sensor performance across the delay period.

The detection and identification system for sensor-bias failure was tested extensively with data from the Heathrow sensor lines. Specific periods were chosen to provide data containing actual sensor failures. The system identified all known sensor failures that had been previously identified by visual pattern recognition of raw data, and no false identifications were made. In addition, the system

identified several sensors which showed marginal performance, which had not been previously identified by visual pattern recognition.

Experience has shown that the most difficult failures to detect and identify are the marginal failures which exceed the 5 ft/sec failure threshold by only a small amount. Typically it takes two to three filter time constants to identify these failures. Larger failures take less time, depending upon the magnitude of the failure. Hence there is a compensatory effect in that the larger the failure, the more quickly it can be identified and hence the shorter the period during which bad data are ingested by the estimator.

4.2 SENSOR NOISE-FAILURE IDENTIFICATION

A procedure similar to the bias-identification process is used to identify excessive random or high-frequency noise in sensor outputs. The 60-second delay after the aircraft identification is again used to eliminate vortex effects. The noise identification procedure calculates sample variances of the sensor outputs and compares them with each other to identify failures.

At sample times other than during the 60-second delay after the aircraft detection, the output of each sensor is squared and the result processed through a first-order low-pass filter. There is one filter associated with each sensor, and the filters are all identical, with time constants of 200 seconds. The output of each filter is a measure of the sample mean-square output of the associated sensor. The sample mean for each sensor, obtained from the sensor bias-failure calculation, is squared and subtracted from the sample mean square for that sensor, to obtain a sample variance for each sensor. The sample variances are then averaged to attain a sample variance for the entire sensor line. Comparisons are then made between the individual sample variances and the average sample variance. The sensor with the largest deviation above 25 $(ft/sec)^2$ is designated as failed and its output eliminated. The average is recalculated and comparisons repeated. Iterations continue until all deviations are less than 25 $(ft/sec)^2$.

This noise-failure identification procedure was also tested extensively with real data from the Heathrow sensor lines. Behavior similar to that of the bias-failure identification system was observed. All failures were correctly identified, no false alarms were issued, and a number of marginal failures which had previously gone undetected were found.

5. COMPUTER REQUIREMENTS

The algorithms developed for vortex tracking and failure identification can be readily applied to a system deployed in the field. The algorithms lend themselves nicely to modularization and thus can be readily implemented in either a central processor or a modular computation system composed of many small, interconnected processors. In order to define the requirements for such a system, the algorithms were analyzed to determine the most useful modular configuration. The following sections describe the various modules and indicate the storage requirements estimated for each module.

5.1 AIRCRAFT DETECTION PROCESSING AND INITIALIZATION FOR NEW AIRCRAFT ARRIVAL

This module processes data from the pressure sensors which are used to indicate aircraft arrival. Certain logical checks are used to reject false alarms. Once it is determined that a new aircraft is present, the program provides initialization of variables in preparation for tracking the new vortices generated by the aircraft. The module is estimated to require 100_{10} words of storage.

5.2 DATA-CONSISTENCY CHECKS AND SCALING

This module does preliminary processing of input data in order to prevent bad-data ingestion by the estimator. It checks for large sensor-data deviations caused by bursts of electrical noise, determines loss of reference voltages and performs any other diagnostic tasks that do not require long-term filtering as utilized in the sensor failure identification system described in Section 4.0. The module also scales sensor data in a manner appropriate for subsequent utilization in the vortex estimator. Storage requirements are estimated at 120_{10} words.

5.3 CLOCK-UPDATE, DATA-OUTPUT, AND EXECUTIVE FUNCTIONS

This module performs various executive functions, including timekeeping, output data processing, and overall system management. Its storage requirement is estimated at 250_{10} words.

5.4 DETERMINATION OF LATERAL POSITION OF SENSORS PRODUCING MAXIMUM OUTPUTS

The maximum sum of two sensor outputs, as described in Section 2.4, and the lateral position of the maximum are determined by this module. A major portion of the module consists of logic for bridging the gap between sensors when a failed sensor is present. Storage requirement is estimated at 200_{10} words.

5.5 DETERMINATION OF LATERAL POSITION OF SENSORS PRODUCING MINIMUM OUTPUTS

This module is essentially the same as 5.4 above, except that it searches for minimum sensor outputs.

5.6 WIND COMPUTATION AND VORTEX PROPAGATION

The estimation of ambient wind velocity is done in this module. The estimate is then utilized to extrapolate vortex estimated position between sample times. Storage requirements for this module are estimated at 80_{10} words.

5.7 DETERMINATION OF MEASURED STARBOARD-VORTEX POSITION AND ESTIMATOR UPDATE

The outputs of sensors producing the maximum output, as determined in 5.4, are used to calculate the measured position of the starboard vortex. This measured position is then processed by the estimator to produce updated starboard vortex position and velocity estimates. Storage requirements for this module are estimated at 175_{10} words.

5.8 DETERMINATION OF MEASURED PORT-VORTEX POSITION AND ESTIMATOR UPDATE

This module is the same as 5.7 except that it performs the same tasks for the port vortex.

5.9 FAILURE IDENTIFICATION

This module implements the sensor's failure-identification routine, as described in Section 4. Storage requirements are estimated at 150_{10} words.

5.10 COMPUTER WORD LENGTH

The variable requiring the largest dynamic range is the vortex location. Its greatest magnitude can be about 500 ft and the resolution should be to within about 10 ft. Hence a dynamic range of 50 is required, implying about 7 binary bits of information plus a sign bit. Hence, an 8-bit processor is sufficient to handle the problem if multiplications are carried out to 16 bits and truncated to 8 bits.

5.11 COMPUTER SPEED

Any modern processor with basic operation times of the order of 10 μsec is sufficiently fast to handle the problem.

6. SIMULATOR PLAN

A portion of the effort expended in this research included the development of a plan for implementing a simulation of the vortex-tracking problem. This simulator will be used to aid in the planning of vortex-tracking systems for airports. The simulator is to be very general, allowing great flexibility in simulating a wide range of tracking situations. Its design is based on a modular approach to developing the various required elements of the system. The modules are chosen in a manner consistent with the various physical phenomena or operational elements that influence vortex tracking. Their size is based on the desire to have each module as self-contained as possible with a minimum of input and output requirements. In the sections that follow, the roles of the various modules will be discussed and the overall simulator system design explained. A diagram of the simulator configuration is presented in Figure 6-1.

6.1 Aircraft Module

The initial locations of vortices are determined by the path flown by the aircraft generating the vortices. This simulation module generates the flight paths of aircraft on approach to landing and on climb-out after takeoff. It effectively provides the initial conditions for the vortex simulation module, which is described in the next section.

The module will also contain a simplified aircraft dynamic simulation along with a closed-loop simulation of the pilot or automatic landing system. The purpose here is to allow some evaluation of the effect of a vortex encounter on an aircraft during final approach or climb-out.

6.2 VORTEX-DYNAMICS MODULE

This module will produce a simulation of vortex motion and determine the velocities produced by the vortices at designated points in space. All important aspects of vortex dynamics will be included so as to provide an accurate representation of the motion. The simulation will be done in three dimensional space, with the locus of vortex centers represented as connected line segments. Vortex motions will be represented by motions of these lines in the three-dimensional space. The initial location and shape of each vortex line is determined by the aircraft simulation program described above. Ground effect, ambient wind, air turbulence, vortex interactions, and vortex decay will all be included by appropriate mathematical modelling.

Also stored within this module will be the geometry of the particular airport being studied. Provision will be made to specify the airport terrain, locations of runways, and placement of vortex sensors. With this data and the lines of vortex centers, as described above, vortex induced velocity at desired points will be generated. In particular, the induced velocities at the locations of the vortex sensors and at nearby runways can be supplied as output from the program.

6.3 SENSOR-SIMULATION MODULE

This module provides mathematical models of the ground-wind anemometers. Its input is the local air velocity at locations of each of the sensors, and its output is indicated velocity, including sensor errors. These errors will include a bias term, scale-factor deviations and a high-frequency noise component. Provision will also be made to simulate misalignment of the sensor relative to its desired orientation.

Simulations of sensor failures will also be implemented in this module. A wide range of possible malfunctions will be provided, in order to allow evaluation of tracking effectiveness in the presence of various failures. The type of failure, magnitude, and time of repair can all be specified by appropriate inputs to the module.

6.4 TRACKING-SYSTEM MODULE

In an actual airport installation the tracking task will be accomplished in a dedicated digital computer system. It is currently envisioned that this computer system will be of modular design, made up of a number of microprocessors tied together by appropriate data communication buses.

The simulator will be designed to allow simulation of this type of system. Both hardware and software will be implemented as elements within the simulator; this will allow evaluation of the data-processing system's hardware configuration as well as checkout of tracking algorithm software. By providing a detailed simulation of the data processing system, it is anticipated that sizable savings in hardware and software costs can be realized by appropriate system checkout on the simulator.

6.5 DATA OUTPUT-AND-DISPLAY MODULE

A very carefully designed data output-and-display system will be utilized to provide simulation results to users. The system will simulate the display system which will be available to air-traffic controllers; its purpose is to inform the controllers of whether there are any vortices within the $\pm$ 150-ft protected region.

This simulator module will also provide users with a versatile means of monitoring variables generated within the simulator, for purposes of evaluating system performance. Users will be able to choose from a series of fixed data formats, which will allow a wide range of choice relative to the amount of detail which will be provided in the output. In addition, provision will be made to allow users to construct a desired output format, which might differ from one of the fixed formats. A very versatile and carefully implemented system for control of data output will be devised.

6.6 EXECUTIVE PROGRAM

The various simulation modules will be tied together through an executive program which will serve to organize the modules, exercize logical decision making, and provide the overall management of the simulator while it is running.

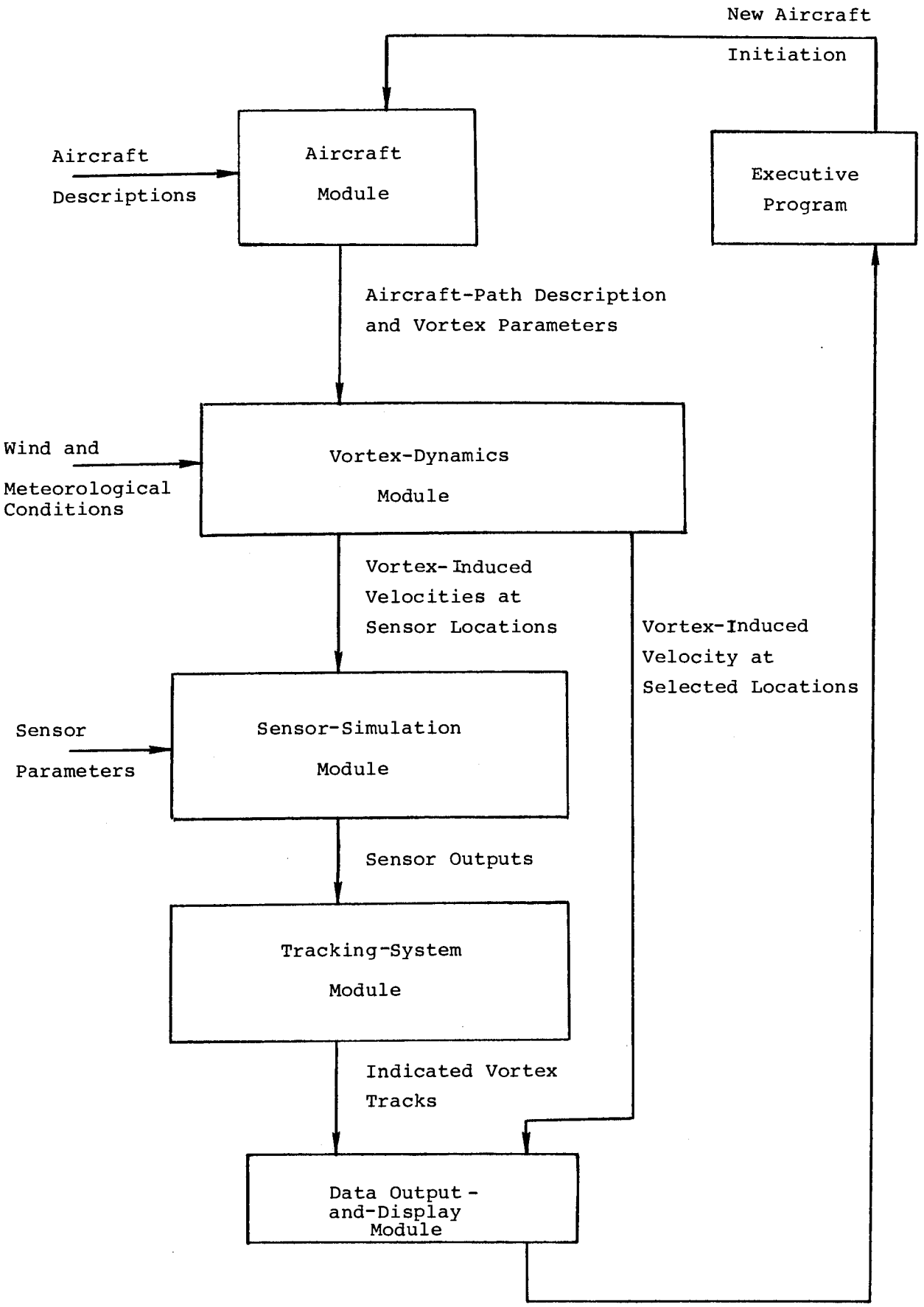

FIGURE 6.1 SIMULATOR CONFIGURATION

7. CONCLUSIONS

An effective, automatic vortex-tracking software system has been developed to process data from ground-wind propeller anemometers. System performance has been verified using actual sensor data gathered at London's Heathrow International Airport. The system works well over large variations in wind conditions and variations in strength of vortices. It is tolerant of sensor errors and adapts readily to loss of sensors due to malfunction.

An effective software system for detecting and identifying sensor failures has also been developed. Actual sensor data were used to verify performance of the failure detection and identification software. All failures previously identified by visual pattern recognition with raw data were also recognized as failures and identified by the automatic system, and no false alarms were given. In addition, certain marginal failures, which had previously gone undetected by visual pattern recognition, were found by the automatic system.

The software has proven itself with actual sensor data under a wide range of operating conditions. It can be readily adapted to real-time tracking and for application to future vortex warning systems installed at airports. Initial steps have been taken to modularize the software, in preparation for its implementation in either a central data processing installation or a modular computer system.

A tentative plan for development of a general-purpose vortex-tracking simulation program has also been presented. This simulator will be an effective tool for the study and development of vortex warning systems. If properly designed, the simulator will be useful for planning sensor installations, software development and verification, performance evaluation, and for studying various combinations of sensor deployment, operational procedures, and sensor-failure detection.

APPENDIX A

DERIVATION OF EQUATION FOR INFERRED VORTEX POSITION MEASUREMENT

A useful equation can be derived for the lateral position of a vortex in terms of three measurements of induced velocity. The equation is based on an assumed $\frac{1}{r}$ velocity field for the vortex induced velocity. From Eq. 2.6 the horizontal velocity measured by sensor i is

$$v_{m_i} = \frac{\Gamma h}{\pi[h^2 + (x-d_i)^2]}, \qquad \text{(A-1)}$$

where

Γ = vortex circulation
h = vortex altitude
x = vortex lateral position
d_i = sensor lateral position.

If there are three sensors, then three equations of the form (A-1) can be written for the three sensors with i = 1, 2, 3. The equations for sensors 1 and 2 can be combined to eliminate $\frac{\Gamma h}{\pi}$, obtaining

$$v_{m_1}\left[\left(h^2+x^2\right) -2d_1x + d_1^2\right] = v_{m_2}\left[\left(h^2+x^2\right) -2d_2x + d_2^2\right], \qquad \text{(A-2)}$$

and similarly for sensors 1 and 3

$$v_{m_1}\left[\left(h^2+x^2\right) -2d_1x + d_1^2\right] = v_{m_3}\left[\left(h^2+x^2\right) -2d_3x + d_3^2\right]. \qquad \text{(A-3)}$$

These two equations can then be combined to eliminate the term (h^2+x^2), obtaining

$$\frac{v_{m_1}-v_{m_2}}{v_{m_1}-v_{m_3}} = \frac{x\left(2d_1v_{m_1}-2d_2v_{m_2}\right)+ v_{m_2}d_2^2 - v_{m_1}d_1^2}{x\left(2d_1v_{m_1}-2d_3v_{m_3}\right)+ v_{m_3}d_3^2 - v_{m_1}d_1^2}, \qquad \text{(A-4)}$$

which can then be solved for x to yield

$$x = \frac{\left[v_{m_1} d_1^2 \left(v_{m_2} - v_{m_3}\right) + v_{m_2} d_2^2 \left(v_{m_3} - v_{m_1}\right) + v_{m_3} d_3^2 \left(v_{m_1} - v_{m_2}\right)\right]}{2\left[v_{m_1} d_1 \left(v_{m_2} - v_{m_3}\right) + v_{m_2} d_2 \left(v_{m_3} - v_{m_1}\right) + v_{m_3} d_3 \left(v_{m_1} - v_{m_2}\right)\right]} \quad . \qquad \text{(A-5)}$$

APPENDIX B

SUBROUTINE SUMMARIES, PROGRAM FLOWCHART, AND PROGRAM LISTINGS

The subroutine summaries are preceded by a glossary. The basic format of each subroutine summary appearing on the following pages is composed of the following terms:

A) Purpose
B) Calling Sequence
C) Inputs
D) Outputs
E) Subroutines Called
F) Subroutine Length
G) Warning or Error Messages.

A flowchart is then enclosed for the significant and complicated subroutines, followed by the FORTRAN listing for each subroutine.

ESTIMATOR-TRACKER GLOSSARY

ABSPL	Absolute value of port-vortex position
ABSPR	Absolute value of starboard-vortex position
ALT	Altitude of port or starboard vortex
C_V	Velocity-filter measurement weight
C_X	Position-filter measurement weight
DELT	Time step
DENOM	Denominator used in calculating the measured lateral position of either the port or starboard vortex
DMN	Locations of the three smallest average-velocity sensors at time N
DMX	Locations of the three largest average-velocity sensors at time N
DN	Lateral positions of the three sensors which represent the minimum average velocity
DSQ	Used to determine if the magnitude of the difference between the measured position and the estimated position is consistent with expected measured and estimated errors
DX	Lateral positions of the three sensors which represent the maximum average velocity
D1	Lateral position of the sensor with the largest velocity for starboard, smallest velocity for port
D2	Lateral position of the sensor with the smallest velocity for starboard, largest velocity for port
I	Index pointer
IBLMN	Indicates that the minimum value for the sum of two sensors is on the left-hand boundary
IBLMX	Indicates that the maximum value for the sum of two sensors is on the left-hand boundary

IBRMN	Indicates that the minimum value for the sum of two sensors is on the right-hand boundary
IBRMX	Indicates that the maximum value for the sum of two sensors is on the right-hand boundary
ICL{O,I}*	Indicator used in termination logic on port side
ICLK	Internal clock used to count frames per second
ICR{O,I}	Indicator used in termination logic on starboard side
IDX	Index pointer
IFST	Indicator used on outer baseline to signal arrival of new aircraft
IFSTI	Indicator used on inner baseline to signal arrival of new aircraft
II	Counter
IPDX	Index pointer
IPX	Index pointer
IS	Sensor number
JJ	Counter
J1	Sensor location on the left-hand side of the minimum or maximum sensor-pair chosen
J2	Sensor location on the left-hand side of the minimum or maximum sensor-pair chosen
J3	Sensor location on the right-hand side of the minimum or maximum sensor-pair chosen
J4	Sensor location on the right-hand side of the minimum or maximum sensor-pair chosen
L	Measured lateral position of the port vortex
LARG	Large floating-point number used for initialization
MNL{O,I}	The location of the first sensor on a baseline
MXR{O,I}	The location of the last sensor on a baseline

---

*O - means outer baseline
I - means inner baseline

NP	Number of sensors minus the number of failed sensors minus three
R	Measured lateral position of the starboard vortex
RMSVW{O,I}*	Root-mean square wind velocity
SCONST	Scaling constant
SECC	Forty-second threshold
SECO	Ten-second threshold
SEC60	Sixty-second threshold
SMALL	Small floating-point number used for initialization
SMAX	Maximum velocity for the sum of two sensors
SMAX3	Strength of the starboard vortex
SMIN	Minimum velocity for the sum of two sensors
SMIN3	Strength of the port vortex
SNLBST	Intermediate variable used to store the largest difference between two successive signal-to-noise ratio values on the port side
SNL{O,I}	Signal to noise ratio for the port vortex
SNLP	Intermediate variable used to store a previous signal-to-noise ratio value on the port side
SNRBST	Intermediate variable used to store the largest difference between two successive signal-to-noise ratio values on the starboard side
SNR{O,I}	Signal-to-noise ratio for the starboard vortex
SNRP	Intermediate variable used to store a previous signal-to-noise ratio value on the starboard side
SPRTL	Print trigger to indicate start of the port-vortex track
SPRTR	Print trigger to indicate start of the starboard-vortex track
SRMSVW	Smoothed root-mean-square wind velocity
SSMN	Smoothed signal-to-noise ratio for the port vortex
SSMX	Smoothed signal-to-noise ratio for the starboard vortex

*O - means outer baseline
I - means inner baseline

SSQVW	Sum of the squares of good sensor velocities, excluding the two sets of sensors with the largest and smallest velocity
SUM	Intermediate variable used to store the maximum or minimum velocity for the sum of two sensors
TEM	Intermediate variable used in the calculation of the measured lateral position
TEMP	Temporary variable
TPIE	Constant
V_L	Velocity estimate of the port vortex
V_R	Velocity estimate of the starboard vortex
V_W	Wind velocity estimate
WOLD	$e^{-\Delta t/\text{Time Constant}}$ used for smoothing old data
WNEW	(1-WOLD) used for smoothing new data
X	Scaled vortex motion as recorded by sensors minus wind estimate
XHAT	Scaled vortex motion

ESTIMATOR-TRACKER SUBROUTINE

A. Purposes

To track automatically, and to record measured vortex positions as a function of time.

B. Calling Sequence

CALL EST (Z, ISPIKE, NS, ISN, ISDST, IORD, METS, NF, P_L, P_R, SSQL, SSQR, SMNL, SMXR, SPRTL, SPRTR)

C. Inputs

Through variables in calling sequence

Z_i	Ground-wind sensor data as recorded by propeller anemometers
ISPIKE	Trigger to indicate spike in GWS data
NS	Total number of sensors in a baseline
ISN_i	Indicates failed sensors in a baseline
$ISDST_i$	Sensor lateral positions in a baseline with respect to the centerline of a runway
$IORD_i$	Sensor locations in a baseline with respect to the centerline of a runway, ordered from port to starboard
$METS_i$	Ambient meteorological wind data recorded at various levels on multiple towers
NF	Total number of failed sensors in a baseline

The remaining inputs are passed through labeled common blocks.

/INOU/ -Specifies input, output, and scatch device numbers.

/INPUT1/, /PASS21/, /ORDER3/ -See glossary for definition of variables in these common blocks.

D. ØUTPUTS

Through variables in calling sequence

P_L	Position estimate of the port vortex
P_R	Position estimate of the starboard vortex
SSQL	Smoothed quality indicator for the port vortex
SSQR	Smoothed quality indicator for the starboard vortex
SMNL	Smoothed strength of the port vortex
SMXR	Smoothed strength of the starboard vortex
SPRTL	Print trigger to indicate start of the port vortex track
SPRTR	Print trigger to indicate start of the starboard vortex track

The remaining outputs are passed through a labeled common block.

/EST{O,I}/ -See glossary for definition of variables in this common block.

E. Subroutines Called

CK, FDI

F. Subroutine Length

1525_8 locations

VORTEX ESTIMATOR TRACKER MODULE

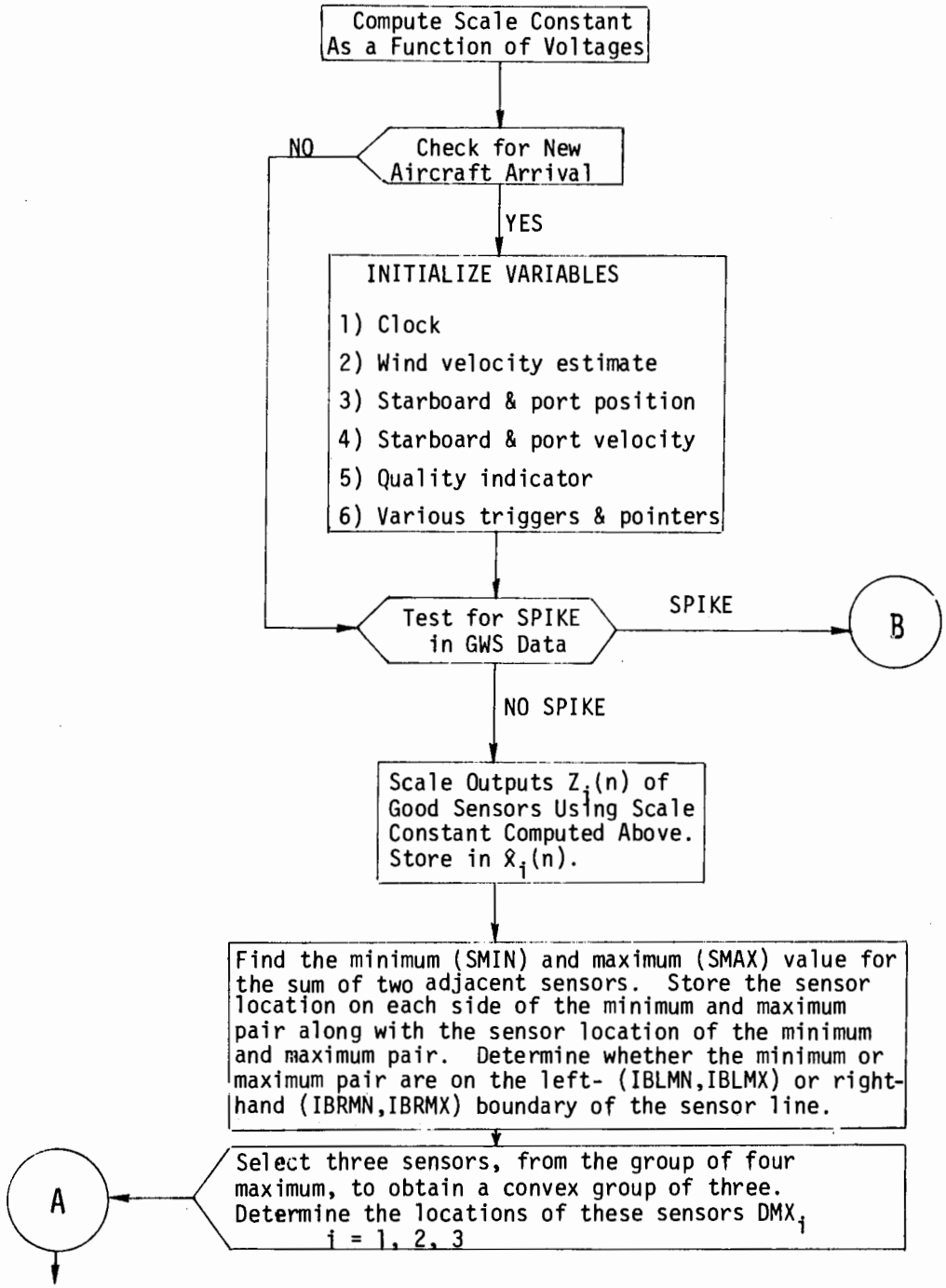

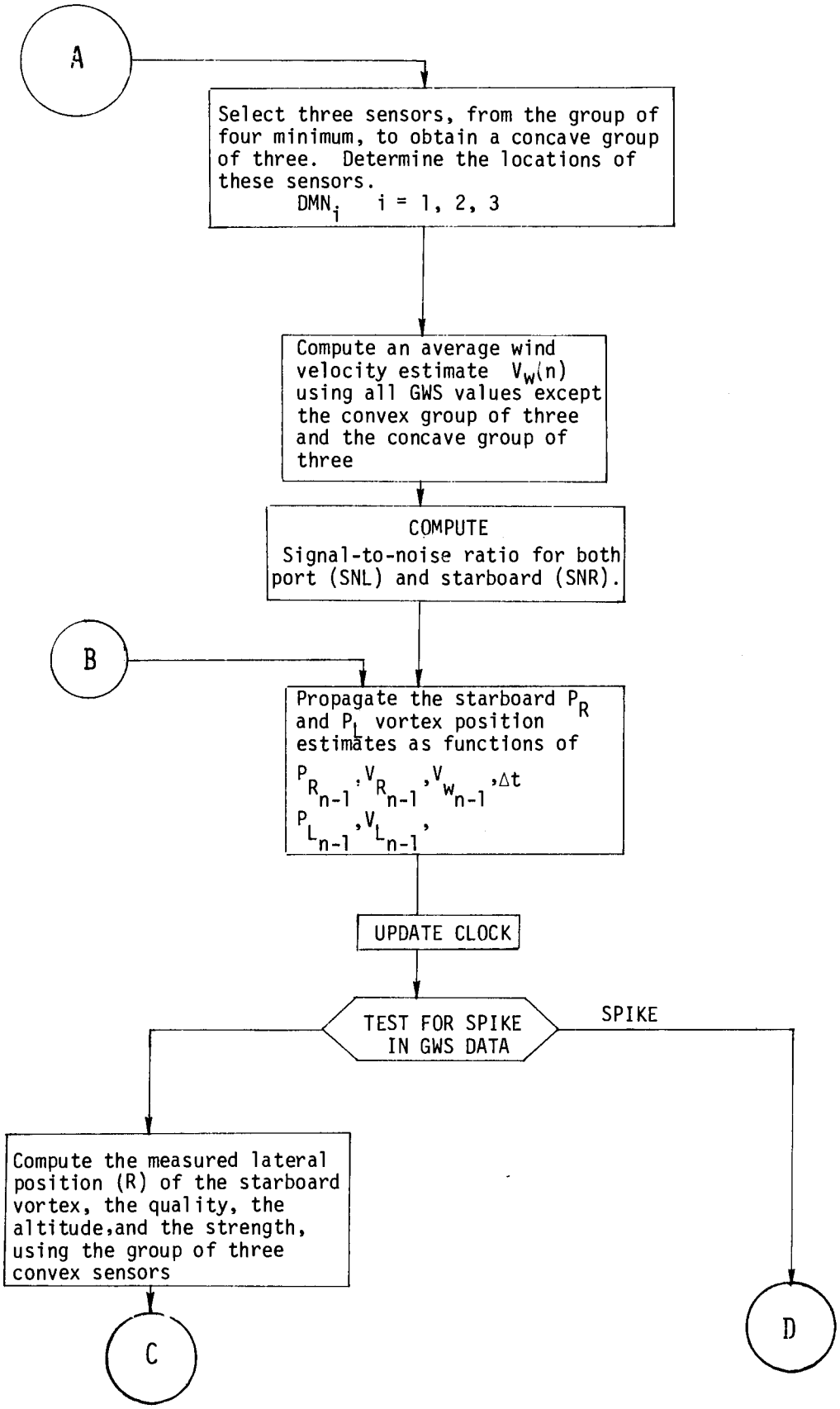
A
Select three sensors, from the group of four minimum, to obtain a concave group of three. Determine the locations of these sensors.
DMN_i i = 1, 2, 3
Compute an average wind velocity estimate $V_w(n)$ using all GWS values except the convex group of three and the concave group of three
COMPUTE
Signal-to-noise ratio for both port (SNL) and starboard (SNR).
B
Propagate the starboard P_R and P_L vortex position estimates as functions of
$P_{R_{n-1}}, V_{R_{n-1}}, V_{w_{n-1}}, \Delta t$
$P_{L_{n-1}}, V_{L_{n-1}}$,
UPDATE CLOCK
TEST FOR SPIKE IN GWS DATA
SPIKE
Compute the measured lateral position (R) of the starboard vortex, the quality, the altitude, and the strength, using the group of three convex sensors
C
D

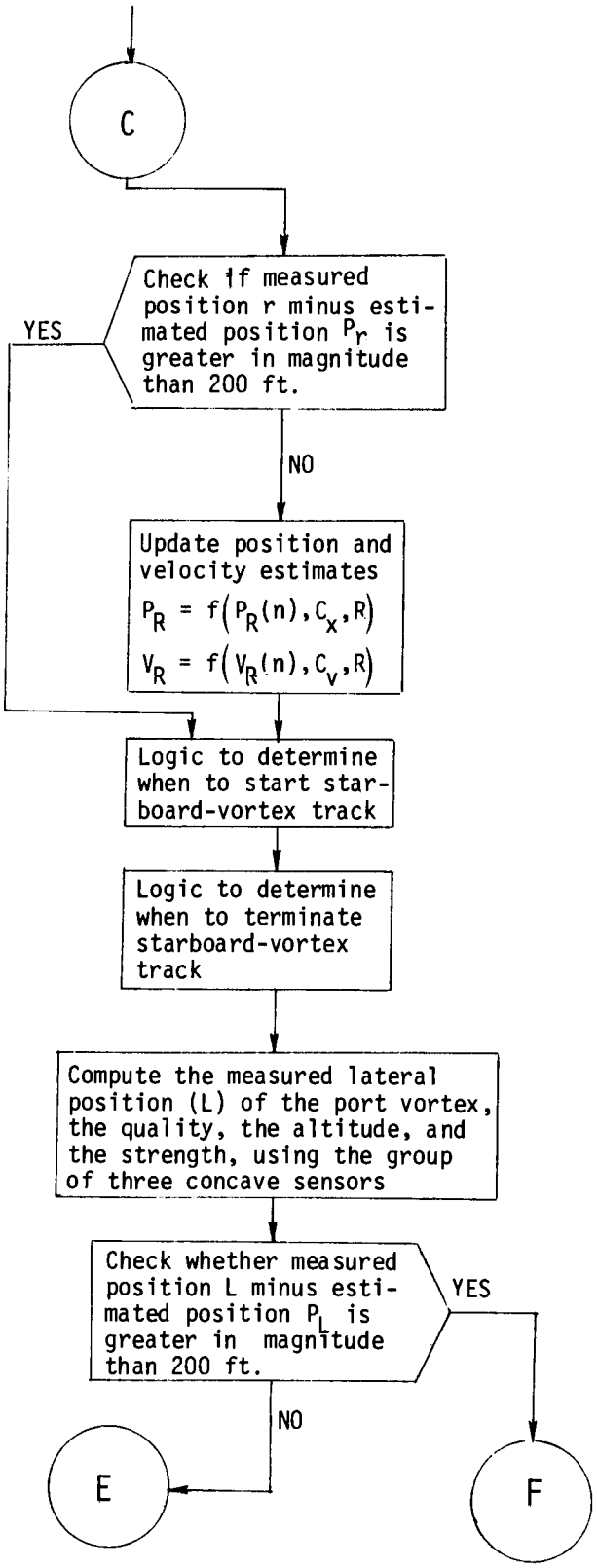
C
Check if measured position r minus estimated position P_r is greater in magnitude than 200 ft.
YES
NO
Update position and velocity estimates
$P_R = f(P_R(n), C_x, R)$
$V_R = f(V_R(n), C_v, R)$
Logic to determine when to start starboard-vortex track
Logic to determine when to terminate starboard-vortex track
Compute the measured lateral position (L) of the port vortex, the quality, the altitude, and the strength, using the group of three concave sensors
Check whether measured position L minus estimated position P_L is greater in magnitude than 200 ft.
YES
NO
E
F

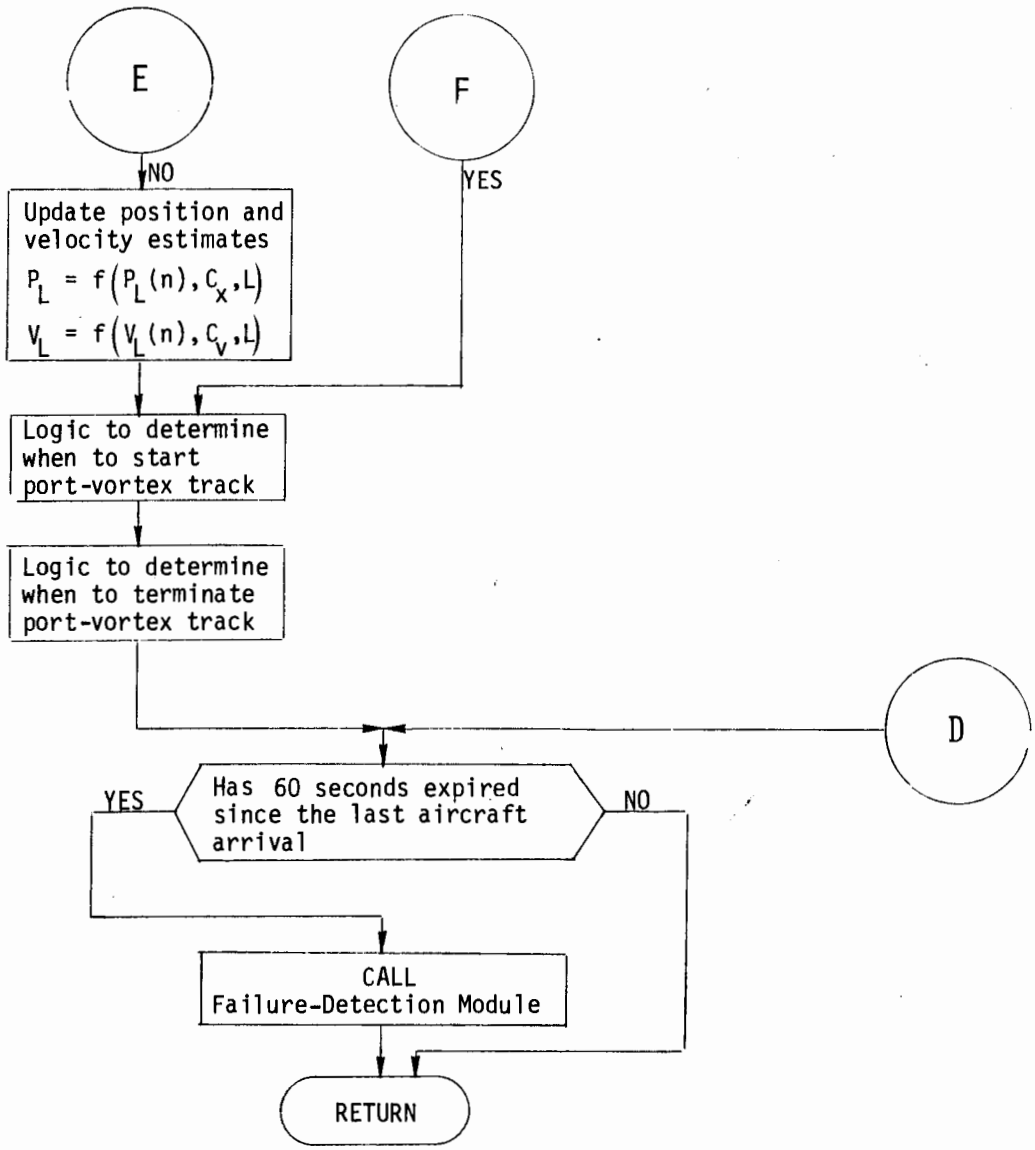
E
F
NO
YES
Update position and velocity estimates
$P_L = f(P_L(n), C_x, L)$
$V_L = f(V_L(n), C_v, L)$
Logic to determine when to start port-vortex track
Logic to determine when to terminate port-vortex track
D
YES
Has 60 seconds expired since the last aircraft arrival
NO
CALL Failure-Detection Module
RETURN

ESTIMATOR-TRACKER SUBROUTINE

```
      SUBROUTINE EST(Z,ISPIKE,NS,ISN,ISDST,ICRD,METS,NF,PL,PR,SSQL,SSQR
     1,SMNL,SMXR,SPRTL,SPRTR)
      REAL L, LARG, M2, M1
      INTEGER DMN, DMX, Z, SECO, SECC, SPRTR, SPRTL, SEC60
      DIMENSION
     1 DN(3), DX(3), DMN(4), DMX(4), TEM(3), X(3), XHAT(30)
      DIMENSION
     1 ISN(30), ISDST(30), IORD(30), METS(10), Z(30)
      COMMON/INOU/ICR,IPR,IPU,IDT,IS1,IS2,ITY,IS3,IS4,IS5,IS6
      COMMON/INPT1/CX,CV,DSQ,DELT,SECO,SECC,WOLD,WNEW
      COMMON/PASS21/IFST,IFST1
      COMMON/ORDER2/MNLO,MXRO
      COMMON/ESTO/RMSVWO,SNLO,SNRC,ICLK,ICRC,ICLO
      DATA SEC60/420/
      DATA LARG/1.E25/
      DATA SMALL/-1.E25/
      DATA TPIE/6.2831853 08/
C     EQUIVALENCE (METS(8),R2)
      SCONST=100.0/(METS(9)-METS(10))
      IF(IFST.NE.1)GO TO 110
C INITIALIZATION FOR EVERY NEW AIRCRAFT ARRIVAL
      DO 100 I=1,NS
      XHAT(I)=0.0
  100 CONTINUE
      VW=0.0
      VR=0.0
      VL=0.0
      PR=50.0
      PL=-50.0
      IFST=0
      ICLK=0
      SSQR=0.0
      SSQL=0.0
      SMNL=0.0
      SMXR=0.0
      SRMSVW=0.0
      SSMX=0.0
      SSMN=0.0
      SNRBST=0.0
      SNLBST=0.0
      SPRTR=0
      SPRTL=0
      ICRO=4
      ICLO=4
  110 IF(ISPIKE.NE.0)GO TO 265
C UPDATE PREFILTER
      DO 120 I=1,NS
      IDX=IORD(I)
      IF(ISN(IDX).EQ.1)GO TO 120
      XHAT(I)=(FLOAT(Z(IDX)-METS(8)))*SCONST
  120 CONTINUE
C FIND MAX AND MIN MEAN VELOCITY MEASUREMENTS
      SMAX=SMALL
      SMIN=LARG
      IBRMX=0
      IBRMN=0
      NP=NS-3-NF
      I=1
      J1=1
  125 IDX=IORD(J1)
      IF(ISN(IDX).EQ.1)GO TO 130
```

```
      GO TO 140
130   IS=J1+1
      CALL CK(IS,ISN,IORD,NS,J1)
140   IDX=IORD(J1+1)
      IF(ISN(IDX).EQ.1)GO TO 150
      J2=J1+1
      GO TO 160
150   IS=J1+2
      CALL CK(IS,ISN,IORD,NS,J2)
160   IDX=IORD(J2+1)
      IF(ISN(IDX).EQ.1)GO TO 170
      J3=J2+1
      GO TO 180
170   IS=J2+2
      CALL CK(IS,ISN,IORD,NS,J3)
180   IDX=IORD(J3+1)
      IF(ISN(IDX).EQ.1)GO TO 185
      J4=J3+1
      GO TO 200
185   IS=J3+2
      CALL CK(IS,ISN,IORD,NS,J4)
200   SUM=XHAT(J2)+XHAT(J3)
      IF(SUM.LE.SMAX)GO TO 205
      SMAX=SUM
      IBLMX=0
      DMX(1)=J1
      DMX(2)=J2
      DMX(3)=J3
      DMX(4)=J4
      IF(I.EQ.1)IBLMX=1
      IF(I.EQ.NP)IBRMX=1
205   IF(SUM.GE.SMIN)GO TO 210
      SMIN=SUM
      IBLMN=0
      DMN(1)=J1
      DMN(2)=J2
      DMN(3)=J3
      DMN(4)=J4
      IF(I.EQ.1)IBLMN=1
      IF(I.EQ.NP)IBRMN=1
210   IF(I.GE.NP)GO TO 215
      I=I+1
      J1=J1+1
      GO TO 125
215   J1=DMX(1)
      J2=DMX(2)
      J3=DMX(3)
      J4=DMX(4)
      IF(XHAT(J3).LE.XHAT(J2))GO TO 220
      DMX(1)=DMX(2)
      DMX(2)=DMX(3)
      DMX(3)=DMX(4)
220   DMX(4)=0
      IF(XHAT(J1).GE.XHAT(J2))GO TO 225
      IBLMX=0
225   IF(XHAT(J4).GE.XHAT(J3))GO TO 227
      IBRMX=0
227   J1=DMN(1)
      J2=DMN(2)
      J3=DMN(3)
      J4=DMN(4)
```

```
      IF(XHAT(J3).GT.XHAT(J2))GO TO 230
      DMN(1)=DMN(2)
      DMN(2)=DMN(3)
      DMN(3)=DMN(4)
  230 DMN(4)=0
      IF(XHAT(J1).LE.XHAT(J2))GO TO 235
      IPLMN=0
  235 IF(XHAT(J4).LE.XHAT(J3))GO TO 240
      IPRMN=0
C UPDATE WIND ESTIMATE
  240 II=1
      JJ=1
      NGS=0
      VW=0.0
      SSQVW=0.0
      DO 250 I=1,NS
      IDX=IORD(I)
      IF(ISN(IDX).EQ.1) GO TO 260
      IF(I.EQ.DMX(II))GO TO 245
      IF(I.EQ.DMN(JJ))GO TO 250
      NGS=NGS+1
      VW=VW+XHAT(I)
      SSQVW=SSQVW+XHAT(I)**2
      GO TO 250
  245 II=II+1
      IF(I.NE.DMN(JJ))GO TO 250
  250 JJ=JJ+1
  260 CONTINUE
      VW=VW/NGS
      RMSVWO=SQRT(SSQVW/NGS-VW**2)
      SRMSVW=WOLD*SRMSVW+WNEW*RMSVWO
      SSMX=WOLD*SSMX+WNEW*(.5*SMAX-VW)
      SSMN=WOLD*SSMN+WNEW*(.5*SMIN-VW)
      SNRO=SSMX/SRMSVW
      SNLO=SSMN/SRMSVW
C PROPAGATE VORTEX STATES
C     V=20.0*(C1+C2*DEL)*DEL
C C1  ASSUMED TO BE 1.0
C C2  ASSUMED TO BE 0.0
  265 PR=PR+(VR+VW)*DELT
      PL=PL+(VL+VW)*DELT
      ICLK=ICLK+1
      IF(ISPIKE.NE.0)GO TO 380
C CALCULATE MEASURED RIGHT(STARBOARD) POSITION
      DO 270 I=1,3
      IPX=DMX(I)
      IPDX=IORD(IPX)
      DX(I)=ISDST(IPDX)
      X(I)=XHAT(IPX)-VW
  270 CONTINUE
      IF(IRDMX.EQ.1.OR.IRLMX.EQ.1)GO TO 305
      R=DX(2)
      IF(X(1).LE.0.0.OR.X(2).LE.0.0.OR.X(3).LE.0.0)GO TO 285
      TEM(1)=X(1)*DX(1)*(X(2)-X(3))
      TEM(2)=X(2)*DX(2)*(X(3)-X(1))
      TEM(3)=X(3)*DX(3)*(X(1)-X(2))
      DENOM=2.0*(TEM(1)+TEM(2)+TEM(3))
      IF(DENOM.EQ.0.0)GO TO 305
      DO 280 I=1,3
      TEM(I)=TEM(I)*DX(I)
  280 CONTINUE
```

```
      R=(TEM(1)+TEM(2)+TEM(3))/DENOM
      M1=X(2)
      D1=DX(2)
      IF(X(1).GT.X(3))GO TO 282
      M2=X(1)
      D2=DX(1)
      GO TO 283
  282 M2=X(3)
      D2=DX(3)
  283 TEMP=(M1*(R-D1)**2-M2*(R-D2)**2)/(M2-M1)
      IF(TEMP.LE.0.0)GO TO 285
      ALT=SQRT(TEMP)
      SMAX3=TPIE*M1*(ALT**2+(R-D1)**2)/(2.0*ALT)
      SMXR=WOLD*SMXR+WNEW*SMAX3
  285 TEMP=(R-PR)**2
      SSQR=WOLD*SSQR+WNEW*TEMP
      IF(SSQR.GT.40000.0)SSQR=40000.0
      IF(TEMP.GT.DSQ)GO TO 295
C UPDATE RIGHT(STARBOARD) POSITION AND VELOCITY ESTIMATE STATES
      TEMP=R-PR
      VR=VR+CV*TEMP
      PR=PR+CX*TEMP
  295 IF(ICLK.LE.SECO)GO TO 300
      IF(ICLK.GT.SECC)GO TO 306
      IF(SNRO.LT.2.0)GO TO 300
      TEMP=SNRO-SNRP
      IF(TEMP.LE.0.0)GO TO 300
      IF(TEMP.LE.SNRBST)GO TO 300
      SPRTR=1
      PR=R
      VR=0.0
      SNRBST=TEMP
  300 SNRP=SNRO
      GO TO 306
C  CALULATE MEASURED LEFT(PORT) POSITION
  305 SSQR=WOLD*SSQR+WNEW*10000.0
  306 IF(ICRO.NE.0.AND.SPRTR.EQ.0)GO TO 310
      ICRO=1
      IF(SNRO.LT.2.0)GO TO 310
      ICRO=2
      IF(ICLK.GT.SECC)GO TO 307
      IF(SSQR.GE.22500.0)GO TO 309
      GO TO 308
  307 IF(SSQR.GE.10000.0)GO TO 310
  308 ICRO=3
      ABSPR=ABS(PR)
      IF(ABSPR.GT.ABS(FLOAT(ISDST(MNLO))).OR.ABSPR.GT.ABS(FLOAT(ISDST(MX
     1 RO))))GO TO 310
      ICRO=0
      GO TO 310
  309 IF(SPRTR.EQ.1)SNRBST=0.0
  310 DO 315 I=1,3
      IPX=DMN(I)
      IPDX=IDRD(IPX)
      DN(I)=ISDST(IPDX)
      X(I)=XHAT(IPX)-VW
  315 CONTINUE
      IF(IBRMN.EQ.1.OR.IBLMN.EQ.1)GO TO 380
      L=DN(2)
      IF(X(1).GE.0.0.OR.X(2).GE.0.0.OR.X(3).GE.0.0)GO TO 345
      TEM(1)=X(1)*DN(1)*(X(2)-X(3))
```

```
      TEM(2)=X(2)*DN(2)*(X(3)-X(1))
      TEM(3)=X(3)*DN(3)*(X(1)-X(2))
      DENOM=2.0*(TEM(1)+TEM(2)+TEM(3))
      IF(DENOM.EQ.0.0)GO TO 380
      DO 340 I=1,3
      TEM(I)=TEM(I)*DN(I)
  340 CONTINUE
      L=(TEM(1)+TEM(2)+TEM(3))/DENOM
      M1=X(2)
      D1=DN(2)
      IF(X(1).GT.X(3))GO TO 342
      M2=X(3)
      D2=DN(3)
      GO TO 343
  342 M2=X(1)
      D2=DN(1)
  343 TEMP=(M1*(L-D1)**2-M2*(L-D2)**2)/(M2-M1)
      IF(TEMP.LE.0.0)GO TO 345
      ALT=SQRT(TEMP)
      SMIN3=TPIE*M1*(ALT**2+(L-D1)**2)/(2.0*ALT)
      SMNL=WOLD*SMNL+WNEW*SMIN3
  345 TEMP=(L-PL)**2
      SSQL=WOLD*SSQL+WNEW*TEMP
      IF(SSQL.GT.40000.0)SSQL=40000.0
      IF(TEMP.GT.DSQ)GO TO 365
C UPDATE LEFT(PORT) POSITION AND VELOCITY ESTIMATE STATES
  360 TEMP=L-PL
      VL=VL+CV*TEMP
      PL=PL+CX*TEMP
  365 IF(ICLK.LE.SECO)GO TO 370
      IF(ICLK.GT.SECC)GO TO 385
      IF(SNLO.GT.-2.0)GO TO 370
      TEMP=SNLO-SNLP
      IF(TEMP.GE.0.0)GO TO 370
      IF(TEMP.GE.SNLBST)GO TO 370
      SPRTL=1
      PL=L
      VL=0.0
      SNLBST=TEMP
  370 SNLP=SNLO
      GO TO 385
  380 SSQL=WOLD*SSQL+WNEW*10000.0
      IF(ISPIKE.NE.0)SSQR=WOLD*SSQR+WNEW*10000.0
  385 IF(ICLO.NE.0.AND.SPRTL.EQ.0)GO TO 390
      ICLO=1
      IF(SNLO.GT.-2.0)GO TO 390
      ICLO=2
      IF(ICLK.GT.SECC)GO TO 387
      IF(SSQL.GE.22500.0)GO TO 389
      GO TO 388
  387 IF(SSQL.GE.10000.0)GO TO 390
  389 ICLO=3
      ABSPL=ABS(PL)
      IF(ABSPL.GT.ABS(FLOAT(ISDST(MNLO))).OR.ABSPL.GT.ABS(FLOAT(ISDST(MX
     1 RO))))GO TO 390
      ICLO=0
      GO TO 390
  388 IF(SPRTL.EQ.1)SNLBST=0.0
  390 IF(ICLK.LT.SEC60)GO TO 400
      CALL EDI(XHAT,NS,ISN,IORD,NF)
  400 RETURN
```

FAILURE DETECTION-AND-IDENTIFICATION SUBROUTINE

A. Purposes

To monitor continuously each sensor's performance, and automatically to identify and to reject failed or poorly performing sensors.

B. Calling Sequence

Call FDI(XHAT,NS,ISN,IORD,NF)

C. Inputs

Through variables in calling sequence

$XHAT_i$	Scaled sensor outputs
NS	Total number of sensors at a baseline
ISN_i	Indicates failed sensors at a baseline
$IORD_i$	Sensor locations at a baseline with respect to the centerline of runway
NF	Total number of failed sensors at a baseline

The remaining inputs are passed through labeled common blocks

/INOU/	Specifies input, output, and scratch device numbers
/INPT3/	Contains constants to filter mean and mean square

D. Outputs

Through labeled common blocks

/VALDO/	Contains filtered mean and filtered mean squared
/FDIO/	Contains filtered variance, total filtered mean, and total filtered variance.

E. Subroutine Length

263_8 locations

F. Warning or Error Messages

a) "SENSOR # "x" ON (OB,IB) EXCEEDS MEAN"

b) "SENSOR # "x" ON (OB,IB) EXCEEDS VARIANCE"

FAILURE DETECTION-AND-IDENTIFICATION SUBROUTINE

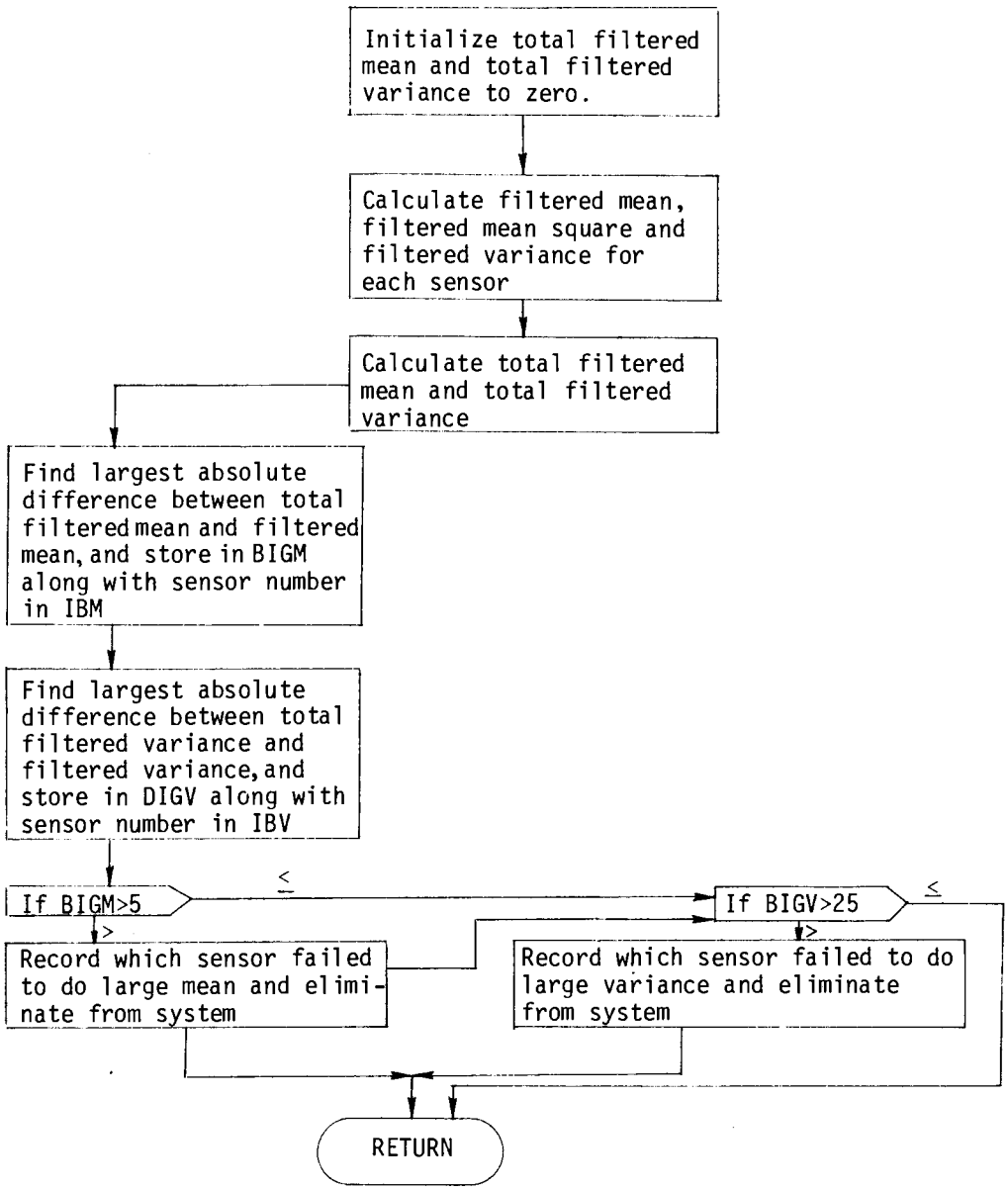

FAILURE DETECTION-AND-IDENTIFICATION SUBROUTINE

```
      SUBROUTINE FDI(XHAT,NS,ISN,IORD,NF)
      REAL MALL
      DIMENSION ISN(30), ISDST(30), IORD(30), METS(10), XHAT(30), Z(30)
      COMMON/INOU/ICP,IPR,IPU,IDT,IS1,IS2,ITY,IS3,IS4,IS5,IS6
      COMMON/INPT3/COLD,CNEW
      COMMON/VALDO/XS(30),YS(30)
      COMMON/FDIO/ZS(30),MALL,VALL
      MALL=0.0
      VALL=0.0
      BIGM=-1.E25
      BIGV=-1.E25
      DO 100 I=1,NS
      IDX=IORD(I)
      IF(ISN(IDX).EQ.1)GO TO 100
      TEM=CNEW*XHAT(I)
      TEMS=TEM*XHAT(I)
   30 XS(I)=COLD*XS(I)+TEM
      YS(I)=COLD*YS(I)+TEMS
      ZS(I)=YS(I)-XS(I)**2
      MALL=MALL+XS(I)
      VALL=VALL+ZS(I)
  100 CONTINUE
      NGS=NS-NF
      MALL=MALL/NGS
      VALL=VALL/NGS
      DO 200 I=1,NS
      IDX=IORD(I)
      IF(ISN(IDX).EQ.1)GO TO 200
      ARGM=ABS(MALL-XS(I))
      IF(ARGM.LE.BIGM)GO TO 150
      IBM=I
      BIGM=ARGM
  150 ARGV=ABS(VALL-ZS(I))
      IF(ARGV.LE.BIGV)GO TO 200
      IBV=I
      BIGV=ARGV
  200 CONTINUE
      IF(BIGM.LE.5.0)GO TO 250
      NF=NF+1
      IDX=IORD(IBM)
      ISN(IDX)=1
      MALL=(FLOAT(NGS)*MALL-XS(IBM))/(NS-NF)
      NGS=NS-NF
      XS(IBM)=0.0
      WRITE(ITY,9000)IBM
  250 IF(BIGV.LE.25.0)GO TO 300
      NF=NF+1
      IDX=IORD(IBV)
      ISN(IDX)=1
      VALL=(FLOAT(NGS)*VALL-ZS(IBV))/(NS-NF)
      NGS=NS-NF
      ZS(IBV)=0.0
      WRITE(ITY,9001)IBV
  300 RETURN
 9000 FORMAT(10H SENSOR ' I2,19H ON OB EXCEEDS MEAN)
 9001 FORMAT(10H SENSOR ' I2,23H ON OB EXCEEDS VARIANCE)
      END
```

CK SUBROUTINE

A. Purpose

To determine the location of the first non-failed sensor in the sensor line.

B. Calling Sequence

Call CK(IS,ISN,IORD,NS,IANS)

C. Inputs

Through variables in calling sequence

IS	Sensor number
ISN_i	Indicates failed sensors at a baseline
$IORD_i$	Sensor locations at a baseline with respect to the centerline of runway
NS	Total number of sensors at a baseline

The remaining inputs are passed through a labeled common block

/INOU/	Specifies input, output and scratch device numbers

D. Outputs

Through variable in calling sequence

IANS	Sensor number of the first non-failed sensor

E. Subroutine Length

50_8 locations

F. Warning or Error Messages

"ERROR IN CK SUB....CHECK FAILED SENSORS...."

SUBROUTINE TO LOCATE FIRST NON-FAIL
SENSOR IN THE SENSOR LINE

```
      SUBROUTINE CK(IS,ISN,IORD,NS,IANS)
      COMMON/INCU/ICR,IPR,IPU,ICT,IS1,IS2,ITY,IS3,IS4,IS5,IS6
      DIMENSION ISN(30),IORD(30)
      DO 100 J=IS,NS
      IDX=IORD(J)
      IF(ISN(IDX).NE.1)GO TO 120
  100 CONTINUE
      WRITE(ITY,1000)
 1000 FORMAT(*0ERROR IN CK SUB....CHECK FAILED SENSORS....*)
      RETURN
  120 IANS=J
      RETURN
      END
```

APPENDIX C

KALMAN FILTER-GAIN EQUATIONS FOR A DOUBLE INTEGRAL PLANT

Consider the double integral plant system described by the following state equations

$$\dot{x}_1 = x_2 , \tag{C-1}$$

$$\dot{x}_2 = u , \tag{C-2}$$

where u is a white Gaussian process noise with the following statistics

$$E[u(t)] = 0 , \quad E[u(t)u(t+\tau)] = q\delta(\tau) , \tag{C-3}$$

and q is the strength of the process noise. Let m(t) be the system output given as

$$m(t) = x_1(t) + v(t) , \tag{C-4}$$

where v(t) is a white Gaussian measurement noise with statistics

$$E[v(t)] = 0 , \quad E[v(t)v(t+\tau)] = r\delta(\tau) , \tag{C-5}$$

with r defined as the strength of the measurement noise.

The object of this development is to obtain the estimator which produces the minimum mean-square error in estimation of x_1 and x_2 from the measurements m. This end can be readily attained by defining the state vector

$$x(t) = \begin{bmatrix} x_1(t) \\ x_2(t) \end{bmatrix} , \tag{C-6}$$

and writing the vector matrix system equations as

$$\dot{x}(t) = Fx(t) + Gu(t), \tag{C-7}$$

$$m(t) = Hx(t) + v(t) , \tag{C-8}$$

where the matrices F, G and H are

$$F = \begin{bmatrix} 0 & 1 \\ 0 & 0 \end{bmatrix}, \tag{C-9}$$

$$G = \begin{bmatrix} 0 \\ 1 \end{bmatrix}, \tag{C-10}$$

$$H = [1 \quad 0] . \tag{C-11}$$

The minimum-error variance estimator is then given by the Kalman filter equations[13]

$$\dot{\hat{x}}(t) = F\hat{x}(t) + K(t)[m(t) - H\hat{x}(t)], \tag{C-12}$$

$$K(t) = \frac{P(t)H^T}{r} , \tag{C-13}$$

where $\hat{x}(t)$ is the estimate of the state vector $x(t)$, as inferred from the available measurement process $m(t)$, $K(t)$ is the matrix of Kalman filter gains and $P(t)$ is the error covariance matrix which satisfies the Riccati equation

$$\dot{P}(t) = FP(t) + P(t)F^T + GqG^T - \frac{P(t)H^THP(t)}{r} . \tag{C-14}$$

Now the vector matrix differential equation for the estimator can be expanded to obtain scalar differential equations for the estimates of the individual elements of the state. These are

$$\dot{\hat{x}}_1(t) = \hat{x}_2(t) + k_1(t)[m(t) - \hat{x}_1(t)], \tag{C-15}$$

$$\dot{\hat{x}}_2(t) = k_2(t)[m(t) - \hat{x}_1(t)], \tag{C-16}$$

where the filter gains $k_1(t)$ and $k_2(t)$ are the first and second elements of the gain matrix given in (C-13),

$$k_1(t) = \frac{p_{11}(t)}{r}, \tag{C-17}$$

$$k_2(t) = \frac{p_{12}(t)}{r}, \tag{C-18}$$

with p_{11} and p_{12} defined as the elements of the covariance matrix $P(t)$.

$$P(t) = \begin{bmatrix} p_{11}(t) & p_{12}(t) \\ p_{12}(t) & p_{22}(t) \end{bmatrix}. \tag{C-19}$$

From Eq. (C-14) the differential equations for the scalar elements of $P(t)$ can be obtained as

$$\dot{p}_{11}(t) = 2p_{12} - \frac{p_{11}^2}{r}, \tag{C-20}$$

$$\dot{p}_{12} = p_{22} - \frac{p_{11}p_{12}}{r}, \tag{C-21}$$

$$\dot{p}_{22} = q - \frac{p_{12}^2}{r}. \tag{C-22}$$

If the filter is allowed to reach steady-state stationary operation, the covariances approach constant values. These can be obtained by setting the left-hand sides of (C-20,21,22) to zero. Eq. (C-22) then yields

$$p_{12} = (qr)^{\frac{1}{2}}, \tag{C-23}$$

and applying this result to Eq. (C-20) obtains

$$p_{11} = 2^{\frac{1}{2}} q^{\frac{1}{4}} r^{\frac{3}{4}}. \tag{C-24}$$

Thus, from Eq. (C-17) and Eq. (C-18) the steady-state filter gains are

$$k_1 = 2^{\frac{1}{2}} \left(\frac{q}{r}\right)^{\frac{1}{4}}, \tag{C-25}$$

REFERENCES

1. Anon., "Aircraft Accident Report: Delta Airlines Inc., McDonnell Douglas DC-9-14 N3305L, Greater Southwest International Airport, Fort Worth, Texas, 30 May 1972," NTSB-AAR-73-3, March 1973, National Transportation Safety Board, Washington DC. (Also, SA-432).

2. Kidd, R. M., "Wake Turbulence - The Invisible Killer," CATCA Journal, Vol. 5, Fall 1973, p. 4-7.

3. Chigier, N. A., "Vortexes in Aircraft Wakes," Scientific American, Vol. 230, No. 3, March 1974, p. 76-83.

4. Gee, D., F. Paillet, and G. Kurylowich, "Analysis of a Wake Turbulence Hazard in USAF Operations (T-39 Accident)." AFFDL-TM-75-19-FGC, Jan. 1975, Air Force Flight Dynamics Laboratory, W.P.A.F.B., OH.

5. Gupta, V. P., "Vortex-Related Accidents Over the Ten Year Period 1964-1973," FAA-EM-75-6, April 1975, MITRE Corp., McLean VA.

6. Hallock, J. N. and W. D. Wood, "Status of the Wake Vortex Avoidance System," EASCON '74 Record, IEEE Electronics and Aerospace Systems Conference, 1974, p. 250-256.

7. Hallock, J. N., "Wake Vortex Decay Near the Ground," AIAA Paper 75-882, Hartford CT, 1975.

8. Hallock, J. N. and L. Goldstone, "US/UK Vortex Monitoring Program at Heathrow Airport," Proceedings of 20th Symposium of Guidance and Control Panel, Plans and Developments for Air Traffic Systems, AGARD, 1975, p. 24-1 to 24-9.

9. Gelb, A. et al, Applied Optimal Estimation, MIT Press, Cambridge MA, 1974, p. 7.

10. Jones, W. P. and H. L. Chevalier, "Aircraft Trailing Vortex Instabilities," International Council of the Aeronautical Sciences Paper 74-34, Haifa, Israel, 1974. (Also, IEEES 600-74-01).

11. Crow, S. C. and E. R. Bate, "Lifespan of Trailing Vortices in a Turbulent Atmosphere," AIAA Journal of Aircraft, July 1976.

12. Tombach, I. H., S. C. Crow, and E. R. Bate, "Investigation of Vortex Wake Stability Near the Ground," AFOSR TR-75-1501, July 1975, Aerovironment Inc., Pasadena, CA.

13. Harlan, R. B., and S. J. Madden, "A Hazard Definition for Wake Turbulence Encounter During Terminal Area Operations," MIT Experimental Astronomy Laboratory Report RE-81, March 1973, MIT, Cambridge MA.